Photogenerated charge collection on diamond electrodes with covalently linked chromophore monolayers
Peer-reviewed author version

Photogenerated charge collection on diamond electrodes with covalently linked chromophore monolayers

J. Raymakers[1]†, A. Artemenko[2]†, F. Verstraeten[1], H. Krysova[3], J. Cermák[2], S. S. Nicley[1], D. Lopez-Carballeira[4], A. Kromka[2], K. Haenen[1], L. Kavan[3], W. Maes[1]*, B. Rezek[4]*

† These authors contributed equally

* Corresponding authors

[1] UHasselt, Institute for Materials Research (IMO) & IMEC vzw, IMOMEC, 3590 Diepenbeek, Belgium

[2] Institute of Physics, Czech Academy of Sciences, 162 00 Prague, Czech Rep.

[3] J. Heyrovsky Institute of Physical Chemistry, Czech Academy of Sciences, 18 223 Prague 8, Czech Rep.

[4] Faculty of Electrical Engineering, Czech Technical University, 166 25 Prague, Czech Rep.

Abstract

Encouraged by its rich surface chemistry and excellent electrochemical properties, boron-doped nanocrystalline diamond (B:NCD) is a promising p-type photoelectrode in dye-sensitized solar cells. One method of diamond surface functionalization using stable carbon-carbon bonds involves the electrochemical grafting of diazonium salts. However, this method typically leads to multilayers that may complicate the transport of photogenerated charges. Here, we establish functionalization of B:NCD electrodes by a monolayer of ethynylphenyl molecules using sterically hindered 4-(trimethylsilyl)ethynylbenzenediazonium tetrafluoroborate. Both the density and structural orientation of the grafted layer are investigated by angular resolved X-ray photoelectron spectroscopy, confirming the presence of covalently grafted monolayers. After removal of the trimethylsilyl protective groups, the resulting ethynyl functionalities are employed to immobilize organic donor-acceptor chromophores via Sonogashira cross-coupling reactions. Homogenous surface coverage is achieved even on the B:NCD electrode. Atomic scale DFT computing reveals that for the chromophore with the strongest acceptor unit, efficient charge separation of 20 Å is obtained where photogenerated holes move directly into diamond. Yet, photocurrent and photovoltage measurements suggest competitive electron recombination to the diamond electrode via the redox electrolyte. Correlation between the density of the molecular layer and photocurrents/photovoltage provides better understanding of the charge generation and recombination pathways in diamond-organic photoelectrochemical cells.

Keywords

1   Introduction

Already in 1955, scientists successfully synthesized artificial diamond from graphite through the high-pressure high-temperature method by mimicking the extreme conditions in the Earth's crust at depths of 160 km.[1] Nevertheless, its practical application remained limited since the crystal size of these man-made diamonds was not bigger than a few millimeters.[2] Progress in the application of synthetic diamond was achieved only after the development of different chemical vapor deposition (CVD) techniques, which allow the synthesis of diamond at low pressure from a gas mixture that typically consists of hydrogen and a carbon source such as methane.[3-5] Nowadays, high quality films of both single crystal and polycrystalline diamond can be readily grown on various substrates[6, 7] and different nanostructures such as nanowires,[8] foams[9] or fibers[10] are accessible. Considering diamond's unique properties, *i.e.* extreme hardness,[11] excellent thermal conductivity,[12] good optical transparency,[13] chemical stability under harsh conditions,[14] wide electrochemical potential window,[15] biocompatibility,[16] tunable electron affinity[17] and the possibility to change diamond from an insulating material to one with semiconducting or even semi-metallic properties upon doping with boron,[18] these diamond materials have been investigated for numerous applications.[19] Boron-doped diamond (BDD) electrodes are currently being employed in commercial chlorine sensors,[20] electrosynthesis,[21] wastewater treatment[22] and the electrocatalytic reduction of CO_2 to CO, formic acid or methanol.[23] Moreover, due to the development of a rich surface chemistry, diamond structures have been decorated with a variety of biomolecules (DNA, proteins, …) and light-harvesting small molecules, resulting in the fabrication of biosensors and dye-sensitized solar cells (DSSCs), respectively.[24, 25]

The application of BDD in p-type DSSCs is appealing since the properties of diamond outperform those of NiO electrodes, which are currently the gold standard in photocathode materials.[26] For instance, diamond's intrinsic chemical inertness is advantageous when corrosive electrolyte solutions such as the I_3^-/I^- redox couple are being employed. BDD also has a high hole diffusion coefficient (2-30 cm^2 s^{-1}), several times larger than that of NiO electrodes (4 x 10^{-8} cm^2 s^{-1}).[27] Even more important is the possibility to functionalize H-terminated diamond surfaces by means of photochemical grafting[28] or diazonium chemistry,[29] resulting in stable carbon-carbon bonds. Subsequently, chromophores can be immobilized on the surface via different types of coupling chemistries.[30-33] In this way, the light-harvesting molecules are anchored onto the electrode material in a fully covalent fashion. These covalent bonds are more robust than the coordination bonds that are employed to functionalize NiO electrodes and should lead to an improved stability at the diamond-chromophore interface.

Pioneering work on the sensitization of BDD electrodes with an electrolyte solution was performed in 1999 by Fujishima *et al.*[34] However, the first covalent functionalization of diamond with bithiophene-C_{60} (2T-C_{60}) through a combination of diazonium grafting and Suzuki cross-cross coupling was only reported a decade later by Zhong *et al.*[35] Optimization of this system resulted in photocurrents of *ca.* 3.5 µA cm^{-1} under 1 sun illumination (100 mW cm^{-2}) in a 5 mM methyl viologen (MV^{2+}) solution.[36] In

3

2014, the Suzuki cross-coupling on phenylboronic acid functionalized diamond thin film electrodes was investigated by Yeap *et al.*, who obtained a surface coverage as high as 0.56 monolayer for the immobilization of a cyclopenta[2,1-*b*:3,4-*b*']dithiophene based chromophore (Br-CPDT-Fur) by employing highly reactive biarylmonodentate phosphine ligands.[30] This functionalized diamond electrode afforded photocurrents of 150 nA cm^{-2} under 0.15 sun illumination (15 mW cm^{-2}) at an external bias of -0.2 V. Translation of this functionalization strategy from thin films to mesoporous diamond foam electrodes resulted in a significant increase of the photocurrent to 15-22 µA cm^{-2}.[37] In previous work we also contributed to the development of diamond-based p-type DSSCs by designing a two-step functionalization approach based on a combination of electrochemical diazonium grafting and Sonogashira cross-coupling.[33, 38] A dithieno[3,2-*b*:2',3'-*d*]pyrrole-2,1,3-benzothiadiazole (DTP-BT) chromophore was immobilized on the diamond surface and photocurrents up to 600 nA cm^{-2} were obtained under 0.9 sun illumination at an applied bias of -0.3 V.[33] A different route to functionalize diamond electrodes with light-harvesting molecules was proposed by Krysova *et al*., using the photochemical grafting of a short terminal alkene (C3) bearing a trifluoroacetamide group. After deprotection, the resulting amine was employed to immobilize 4-(bis(4-[5-(2,2-dicyanovinyl)thiophene-2-yl]phenyl)amino) benzoic acid chloride, also known as the "P1 dye".[39] The photocurrents compared favorably to a non-covalent approach for the same dye.[32] More recently, record currents of 6.6 µA cm^{-2} on thin films were reported by decreasing the amount of boron in the gas feed from 4000 to 250 ppm B/C, which results in a doping concentration (1 x 10^{20} cm^{-3}) slightly below the threshold for semi-metallic conductivity.[40]

Diazonium grafting is commonly employed to introduce various functional groups on the diamond surface. This method was developed in 1999 by Swain *et al.* and holds several advantages over the photochemical approach.[29] The grafting procedure is mostly performed electrochemically by submerging a BDD electrode in a solution of an aryldiazonium salt and cycling to negative potentials. In this manner, the diazonium salt is reduced to its corresponding radical, which is then subsequently grafted on the surface, resulting in a complete passivation after only one cycle. π-π stacking between the aromatic rings contributes to the formation of denser layers.[41] Fully conjugated systems are thought to be beneficial for charge transfer.[35] Nevertheless, electrochemical diazonium grafting also suffers from a major drawback, which is the lack of control and strong tendency to form thick multilayers (5 to 10 nm) due to the attack of radicals on the already grafted layer.[42-44] Since the amount of radicals is directly related to the charge passing through the electrode, multilayer formation can be suppressed by briefly applying a constant potential just below the redox potential of the diazonium salt.[45] H-terminated diamond can also be functionalized with a monolayer through spontaneous diazonium grafting as a result of its intrinsic p-type surface conductivity due to surface transfer doping.[46] Another way to prevent multilayer formation was proposed by Leroux *et al*. and employs diazonium salts that bear bulky functional groups such as triisopropylsilyl protected ethynyl moieties, as they sterically shield the reactive *ortho* positions.[47] However, neither of these precautions against multilayer formation were taken in earlier work by our group during the sensitization of the BDD electrodes.[33, 38] Therefore, it is safe to

4

assume that in all previous cases a multilayer network of a few nanometers exists in between of the chromophores and the diamond electrode. Hence, after excitation of the chromophores, the generated holes have to travel through this layer before they can be injected into the BDD electrode, increasing the chance of charge recombination.

In this work we aimed to functionalize boron-doped nanocrystalline diamond (B:NCD) with a monolayer of ethynylphenyl molecules by employing trimethylsilyl (TMS) protected 4-ethynylbenzenediazonium tetrafluoroborate. These TMS protected diazonium salts were chosen over the more bulky triisopropylsilyl derivatives to obtain a denser layer and a higher surface coverage.[48] The surface composition was thoroughly analyzed to confirm the presence of this monolayer, which until now has only been assumed for B:NCD electrodes. After removal of the protecting TMS groups, three different donor-acceptor chromophores, with increasing electron-deficient character of the acceptor unit, were immobilized onto the surface via Sonogashira cross-coupling. Afterwards, the surface composition was compared with the inverted Sonogashira cross-coupling approach from our previous study[33] and photoelectrochemical and photovoltage measurements were performed to study the influence of this monolayer functionalization on photocurrent generation and charge separation.

2   Materials and methods

2.1   Materials and instrumentation

All purchased chemicals were of the highest available quality and they were used without further purification. 2-Iodothiophene, 4-iodoaniline, ammonium diethyldithiocarbamate, copper(I) iodide, *tert*-butyl nitrite, malononitrile, boron trifluoride etherate, 2-dicyclohexylphosphino-2',6'-dimethoxybiphenyl (SPhos) and 2-dicyclohexylphosphino-2',4',6'-triisopropylbiphenyl (XPhos) were purchased from Sigma Aldrich. Chloroform, dichloromethane, hexanes, dry tetrahydrofuran (THF), dry *N,N*-dimethylformamide (DMF), dry toluene, dry diisopropylamine (DIPA), *n*-butyl lithium (2.5 M solution in *n*-hexane; *n*-BuLi), trimethyltin chloride, tetrabutylammonium fluoride (1.0 M solution in THF; TBAF) and glacial acetic acid were purchased from Acros Organics. *N*-iodosuccinimide, (trimethylsilyl)acetylene and (+/-)-2,2'-bis(diphenylphosphino)-1,1'-dinaphthalene (BINAP) were purchased from Fluorochem. Tris(dibenzylideneacetone)dipalladium(0), tetrakis(triphenylphosphine)palladium (0), *tri*(ortho-tolyl)phosphine, *trans*-dichlorobis(triphenylphosphine)palladium(II) and palladium(II) acetate were purchased from Strem Chemicals. All solvents employed for rinsing were of HPLC grade. DTP **1** and the BT derivatives **2** and **5** were synthesized according to literature procedures.[33, 49, 50]

Preparative (recycling) size exclusion chromatography (prep-SEC) was performed on a JAI LC-9110 NEXT system equipped with JAIGEL 1H, 2H and 3H columns (eluent CHCl$_3$, flow rate 3.5 mL min^{-1}). Nuclear magnetic resonance (NMR) chemical shifts (δ, in ppm) were determined relative to the residual CHCl$_3$ (7.26 ppm) absorption or the ^{13}C resonance shift of CDCl$_3$ (77.16 ppm). High resolution electrospray ionization mass spectrometry (ESI-MS) was performed using an LTQ Orbitrap Velos Pro mass spectrometer equipped with an atmospheric pressure ionization source operating in the nebulizer assisted

electrospray mode. The instrument was calibrated in the *m/z* range 220−2000 using a standard solution containing caffeine, MRFA and Ultramark 1621. UV-Vis absorption spectroscopy measurements were performed on a VARIAN Cary 5000 UV-Vis spectrophotometer at a scan rate of 600 nm min^{-1}. The films for the UV-Vis absorption measurements were prepared by drop casting solutions of the chromophores in chloroform on a quartz substrate. The solid-state UV-Vis absorption spectra were used to estimate the optical gap (from the wavelength at the intersection of the tangent line drawn at the low energy side of the absorption spectrum with the baseline: E_g (eV) = 1240/(wavelength in nm)). Electrochemical measurements (cyclic voltammetry) were performed with an Eco Chemie Autolab PGSTAT 30 potentiostat/galvanostat using a three-electrode microcell with a platinum working electrode, a platinum counter electrode and a Ag/AgNO$_3$ reference electrode (silver wire dipped in a solution of 0.01 M AgNO$_3$ and 0.1 M NBu$_4$PF$_6$ in anhydrous acetonitrile). The reference electrode was calibrated against ferrocene/ferrocenium as an external standard. Samples were prepared by dip coating the platinum working electrode in the chromophore solution. The CV measurements were done on the resulting films with 0.1 M NBu$_4$PF$_6$ in anhydrous acetonitrile as electrolyte solution. To prevent air from entering the system, the experiments were carried out under a curtain of argon. Cyclic voltammograms were recorded at a scan rate of 100 mV s^{-1}. For the conversion of V to eV, the onset potentials of the first oxidation/reduction peaks were used and referenced to ferrocene/ferrocenium, which has an ionization potential of −4.98 eV vs vacuum.

X-ray photoelectron spectroscopy (XPS) was used to determine the chemical composition of the diamond surfaces using an XPS spectrometer (Kratos, AXIS Supra) equipped with a hemispherical analyzer and a monochromatic Al Kα X-ray source (1486.6 eV). The XPS spectra were acquired from an area of 0.7 × 0.3 mm^2 with a takeoff angle of 90°. The survey XPS spectra were recorded with a pass energy of 80 eV, whereas the high-resolution spectrum scans were recorded with a pass energy of 20 eV. The obtained XPS spectra were calibrated on 283.8 eV binding energy (sp^3 carbon phase).[39] The relative atomic concentrations of the chemical elements were calculated from high resolution XPS spectra. The CasaXPS software with implemented linear baseline and Gaussian line shapes was used for spectral processing. XPS peak positions were determined with an accuracy of ±0.2 eV.

All geometry optimizations have been performed gas phase within Density Functional Theory (DFT).[51, 52] A BLYP functional in combination with the 6-31G basis set was used to obtain the structures,[53, 54] while singlet point calculations were carried out with the B3LYP functional,[54, 55] the same basis set and the RIJCOSX approach. This level of theory was also coupled with time-dependent density functional theory (TDDFT).[56] All the wavefunctions were obtained with the ORCA suite of programs and further analyzed with the Multiwfn package.[57]

Macroscopic Kelvin Probe measurements were performed on a Scanning Kelvin Probe system (KP Technologies) using a gold coated probe (tip of 2 mm in diameter) at a distance defined by a gradient of 300. Illumination was provided by a solar simulator, Solar LightLine A1 from Sciencetech Inc. The light

was introduced to the sample via a light guide, of which the end was placed at a distance of 190 mm from the measurement area so that the illumination corresponds to an AM 1.5 solar spectrum.

Photoelectrochemical current measurements were performed in an Ar-saturated 0.1 M Na_2SO_4 solution containing 5 mM methyl viologen (MV^{2+}) as an electron carrier in a three-electrode glass cell equipped with a quartz optical window for illumination of the B:NCD working electrode. The counter electrode was platinum and the reference electrode was Ag/AgCl (sat. KCl). The glass cell was placed in a dark room and controlled by a potentiostat (Zahner, Germany). The white light source was an Oriel LSH – 7320 ABA LED solar simulator. The incident white light intensity was 100 mW cm^{-2} (which is roughly 1 sun).

2.2 Chromophore synthesis

4-(Trimethylsilylethynyl)aniline:[58] 4-Iodoaniline (2.00 g, 9.13 mmol), Pd(PPh$_3$)$_2$Cl$_2$ (0.32 g, 0.27 mmol) and CuI (0.087 g, 0.46 mmol) were loaded in a Schlenk vial equipped with a magnetic stirring bar under inert atmosphere (Ar). Dry THF (30 mL) and dry DIPA (10 mL) were introduced and the mixture was purged with Ar for 30 min before adding trimethylsilylacetylene (2.58 mL, 18.3 mmol). After heating overnight at 50 °C, water (75 mL) was added and the product was extracted with chloroform (3 x 75 mL). The organic phase was dried over MgSO$_4$, filtered and concentrated *in vacuo*. The crude product was purified via column chromatography (silica, hexanes:dichloromethane, 50:50), yielding the product as a brown solid (1.53 g, 88%).

4-(Trimethylsilylethynyl)benzenediazonium tetrafluoroborate:[58] A solution of 4-(trimethylsilylethynyl)aniline (0.772 g, 4.08 mmol) in dry THF (15 mL) was added dropwise to boron trifluoride etherate (2.01 mL, 16.3 mmol) at -20 °C under an inert atmosphere. Subsequently a solution of *tert*-butyl nitrite (1.94 mL, 16.3 mmol) in dry THF (15 mL) was added over 30 min at -20 °C. After stirring for 10 min at -20 °C, the reaction mixture was brought to 5 °C over 20 min. Cold diethyl ether (75 mL) was added and after cooling in an ice-water bath for 15 min, the product was collected as a pale brown solid through filtration (1.02 g, 87%).

4-Hexyl-2-(trimethylstannyl)-4*H*-dithieno[3,2-*b*:2',3'-*d*]pyrrole: *n*-BuLi (2.5 M solution in *n*-hexane; 1.67 mL, 4.18 mmol) was added dropwise to a solution of DTP **1** (1.00 g, 3.80 mmol) in THF (10 mL) at -78 °C. After stirring for 1 h at -78 °C, trimethylstannyl chloride (1.0 M solution in *n*-hexane, 4.75 mL, 4.75 mmol) was rapidly added and the reaction mixture was gradually brought to room temperature. After stirring overnight, water (50 mL) was added and the aqueous layer was extracted with diethyl ether (3 × 50 mL). The combined organic layers were dried over MgSO$_4$, filtered and concentrated *in vacuo*. The crude material was purified via prep-SEC (chloroform), yielding the product as a gray-green oil (1.26 mg, 78%). ^{1}H NMR (400 MHz, Chloroform-*d*): δ = 7.10 (d, *J* = 5.3 Hz, 1H), 7.02 (s, 1H), 6.99 (d, *J* = 5.3 Hz, 1H), 4.19 (t, *J* = 7.1 Hz, 2H), 1.90-1.81 (m, 2H), 1.37-1.23 (m, 6H), 0.87 (t, *J* = 7.1 Hz, 3H), 0.41 (s, 9H).

2-(Benzo[2,1,3]thiadiazol-4-yl)-4-hexyl-4*H*-dithieno[3,2-*b*:2',3'-*d*]pyrrole (3): Monostannylated DTP (1.00 g, 2.35 mmol), monobrominated BT **2** (530 mg, 2.46 mmol), Pd$_2$(dba)$_3$ (64 mg, 0.070 mmol)

and P(o-tolyl)$_3$ (86 mg, 0.28 mmol) were loaded in a Schlenk vial and placed under Ar atmosphere. Next, dry toluene (10 mL) and dry DMF (4 mL) were added, and the mixture was purged with Ar. After refluxing for 1 h, diethyl ether (100 mL) was added and the mixture was washed with water (2 × 100 mL) and brine (50 mL). The organic layer was dried over MgSO$_4$, filtered and concentrated *in vacuo*. The crude product was purified via column chromatography (silica, hexanes:dichloromethane, 60:40), yielding the product as a red solid (930 mg, 95%). ^{1}H NMR (400 MHz, Chloroform-*d*): δ = 8.34 (s, 1H), 7.86 (dd, *J* = 8.7, 0.9 Hz, 1H) 7.84 (dd, *J* = 7.2, 0.9 Hz, 1H), 7.61 (dd, *J* = 8.7, 7.2 Hz, 1H), 7.20 (d, *J* = 5.3 Hz, 1H), 7.02 (d, *J* = 5.3 Hz, 1H), 4.29 (t, *J* = 7.0 Hz, 2H), 1.96-1.88 (m, 2H), 1.39-1.23 (m, 6H), 0.87 (t, *J* = 7.0 Hz, 3H).

2-(Benzo[2,1,3]thiadiazol-4-yl)-4-hexyl-6-iodo-4*H*-dithieno[3,2-*b*:2',3'-*d*]pyrrole (4): *N*-iodosuccinimide (555 mg, 2.47 mmol) was added to a solution of compound **3** (930 mg, 2.35 mmol) in acetic acid (40 mL) and chloroform (40 mL). The reaction mixture was shielded from light and left to stir for 3 h, after which water (75 mL) and chloroform (75 mL) were added. The organic layer was washed with a 20% Na$_2$S$_2$O$_7$ solution (3 × 75 mL), water (2 × 75 mL) and brine (75 mL). Next, the organic layer was dried over MgSO$_4$, filtered and concentrated *in vacuo*. The crude product was purified via column chromatography (silica, hexanes:dichloromethane, 60:40), yielding the product as a red solid (927 mg, 75%). ^{1}H NMR (400 MHz, Chloroform-*d*): δ = 8.29 (s, 1H), 7.87 (dd, *J* = 8.7, 0.9 Hz, 1H), 7.82 (dd, *J* = 7.1, 0.9 Hz, 1H), 7.60 (dd, *J* = 8.7, 7.2 Hz, 1H), 7.20 (s, 1H), 4.22 (t, *J* = 7.1 Hz, 2H), 1.95-1.85 (m, 2H), 1.40-1.24 (m, 6H), 0.87 (t, *J* = 6.4 Hz, 3H); ^{13}C NMR (100 MHz, Chloroform-*d*): δ = 156.3, 152.6, 147.7, 145.4, 137.6, 130.3, 129.1, 124.8, 120.9, 120.0, 119.9, 115.8, 113.3, 72.1, 48.1, 32.1, 31.0, 27.3, 23.2, 14.7; MS (ESI$^+$) Calcd. for C$_{20}$H$_{18}$IN$_3$S$_3$ [M]$^+$: *m/z* 522.9708, found: 522.9703.

7-(4-Hexyl-4*H*-dithieno[3,2-*b*:2',3'-*d*]pyrrol-2-yl)benzo-2,1,3-thiadiazole-4-carbaldehyde (6): Monostannylated DTP (1.00 g, 2.35 mmol), formylated BT **5** (570 mg, 2.35 mmol), Pd$_2$(dba)$_3$ (54 mg, 0.059 mmol) and P(o-tolyl)$_3$ (71 mg, 0.23 mmol) were loaded in a Schlenk vial and placed under Ar atmosphere. Next, dry toluene (10 mL) and dry DMF (4 mL) were added, and the mixture was purged with Ar. After refluxing for 1 h, diethyl ether (100 mL) was added and the mixture was washed with water (2 × 100 mL) and brine (50 mL). The organic layer was dried over MgSO$_4$, filtered and concentrated *in vacuo*. The crude product was purified via column chromatography (silica, hexanes:dichloromethane, 20:80), yielding the product as a purple solid (844 mg, 85%). ^{1}H NMR (400 MHz, Chloroform-*d*) δ 10.66 (s, 1H), 8.53 (s, 1H), 8.19 (d, *J* = 7.6 Hz, 1H), 7.95 (d, *J* = 7.6 Hz, 1H), 7.28 (d, *J* = 5.3 Hz, 1H), 7.02 (d, *J* = 5.3 Hz, 1H), 4.29 (t, *J* = 7.0 Hz, 2H), 1.94 (p, *J* = 7.0 Hz, 2H), 1.42-1.26 (m, 6H), 0.86 (t, *J* = 7.1 Hz, 6H).

7-(4-Hexyl-6-iodo-4*H*-dithieno[3,2-*b*:2',3'-*d*]pyrrol-2-yl)benzo-2,1,3-thiadiazole-4-carbaldehyde (7): *N*-iodosuccinimide (491 mg, 2.18 mmol) was added to a solution of compound **6** (844 mg, 1.98 mmol) in acetic acid (40 mL) and chloroform (40 mL). The reaction mixture was shielded from light and left to stir for 3 h, after which water (75 mL) and chloroform (75 mL) were added. The organic layer was washed with a 20% Na$_2$S$_2$O$_7$ solution (3 × 75 mL), water (2 × 75 mL) and brine (75

mL). Next, the organic layer was dried over $MgSO_4$, filtered and concentrated *in vacuo*. The crude product was purified via column chromatography (silica, hexanes:dichloromethane, 20:80), yielding the product as a purple solid (991 mg, 91%). ^1H NMR (400 MHz, Chloroform-*d*) δ 10.68 (s, 1H), 8.49 (s, 1H), 8.19 (d, *J* = 7.6 Hz, 1H), 7.94 (d, *J* = 7.6 Hz, 1H), 7.22 (s, 1H), 4.24 (t, *J* = 7.1 Hz, 2H), 1.91 (p, *J* = 7.0 Hz, 2H), 1.41-1.27 (m, 6H), 0.91-0.82 (m, 3H). ^{13}C NMR (100 MHz, Chloroform-*d*) δ 188.3, 154.1, 152.3, 146.3, 145.6, 136.2, 134.4, 132.7, 124.9, 122.8, 120.4, 119.7, 118.1, 114.9, 73.9, 47.7, 31.4, 30.3, 26.7, 22.5, 14.0; MS (ESI$^+$) Calcd. for $C_{21}H_{18}IN_3OS_3$ [M + Na]$^+$: *m/z* 573.9554, found: 573.9548.

2-((7-(4-Hexyl-6-iodo-4*H*-dithieno[3,2-*b*:2',3'-*d*]pyrrol-2-yl)benzo-2,1,3-thiadiazole-4-yl)methylene)malononitrile (8): A solution of compound **7** (400 mg, 0.72 mmol), malononitrile (192 mg, 2.90 mmol) and 3 drops of piperidine in dichloromethane (30 mL) was stirred for 90 min at room temperature. The crude mixture was purified via column chromatography (silica, dichloromethane), yielding the product as a metallic green solid (320 mg, 74%) that gives a blue solution in chloroform. ^1H NMR (400 MHz, Chloroform-*d*) δ 8.75 (s, 1H), 8.73 (d, *J* = 8.1 Hz, 1H), 8.49 (s, 1H), 7.93 (d, *J* = 8.1 Hz, 1H), 7.22 (s, 1H), 4.23 (t, *J* = 7.1 Hz, 2H), 1.91 (p, *J* = 6.8 Hz, 2H), 1.39-1.26 (m, 6H), 0.87 (t, *J* = 6.9 Hz, 3H); MS (ESI$^+$) Calcd. for $C_{24}H_{18}IN_5S_3$ [M]$^+$: *m/z* 598.9769, found: 598.9742.

2.3 Diamond growth

150 nm thick B:NCD films were grown on (100)-oriented 10×10^2 mm Si *p*-type conductive substrates by MWPECVD, using trimethylborane (TMB) as the boron source, according to previously employed protocols.[38] Characterization performed on samples grown in the same reactor under similar growth conditions indicated that the B:NCD films have boron concentrations of approximately 5×10^{21} cm^{-3} and a resistivity below 0.005 Ω cm.

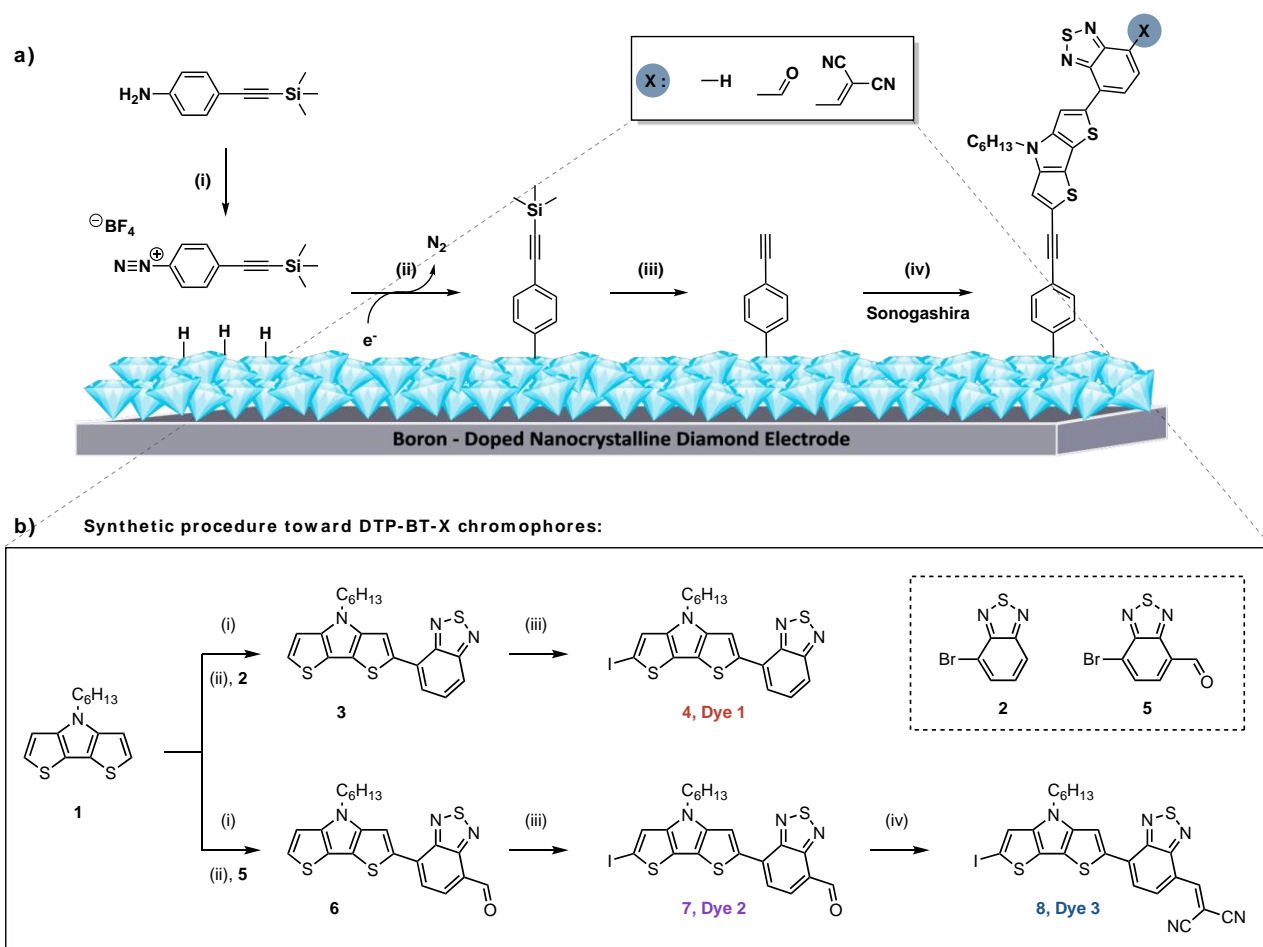## 2.4 Electrochemical diazonium grafting

The B:NCD thin films were functionalized with 4-(trimethylsilyl)ethynylbenzenediazonium tetrafluoroborate by means of electrochemical diazonium grafting using cyclic voltammetry. The electrografting protocol was performed with an Autolab PGSTAT30 potentiostat (Eco Chemie B.V.) and controlled by the GPES Manager software. A one-compartment electrochemical cell was employed in a three-electrode configuration. Hydrogen-terminated B:NCD was used as the working electrode, a platinum wire as the counter electrode and a Ag/AgCl/KCl(sat) electrode as the reference. All potentials are reported versus this reference electrode at room temperature. Diamond working electrodes were functionalized in two steps by immersing each half of the sample in a 4-(trimethylsilyl)ethynylbenzenediazonium tetrafluoroborate solution. The electrografting process was performed by cycling the potential between +600 and -760 mV vs. Ag/AgCl at a scan rate of 50 mV s^{-1} for five scans. After grafting, the B:NCD samples were sonicated in MilliQ water and subsequently rinsed with toluene, THF, ethanol and MilliQ water.

2.5 Sonogashira cross-coupling

All Sonogashira cross-coupling reaction mixtures were prepared in a glovebox under inert atmosphere (N$_2$). The light-harvesting molecule, palladium catalyst, copper(I) iodide, diamond substrate, base and solvent were loaded in a tailor made Schlenk vial equipped with a magnetic stirring bar.[33] The Schlenk vial was closed off with a rubber septum, removed from the glovebox and placed in an oil bath at 60 °C for 16 h. After surface functionalization, all B:NCD samples were sonicated in toluene (p.a.), a solution of ammonium diethyldithiocarbamate (25 mg) in THF (10 mL), THF, ethanol and MilliQ water, before drying under a vigorous stream of nitrogen. Specific reaction conditions are given in **Table 3** and **S2**.

3 Results and discussion

The B:NCD functionalization was performed in three steps, as illustrated in **Scheme 1 a**. In the first step, the formation of a monolayer is achieved via the electrochemical diazonium grafting of 4-(trimethylsilyl)ethynylbenzenediazonium tetrafluoroborate (TEBDT). After removal of the TMS protecting groups, the resulting ethynylphenyl terminated diamond surface can be employed to covalently link iodine functionalized chromophores via Sonogashira cross-coupling reactions.

Scheme 1 | a. General B:NCD functionalization strategy for the development of diamond photocathodes: (i) Diazotization of 4-(trimethylsilyl)ethynylaniline; (ii) Electrochemical reduction and subsequent grafting of the corresponding diazonium salt; (iii) Removal of the trimethylsilyl groups with

tetrabutylammoniumfluoride (TBAF); (iv) Dye sensitization of diamond via Sonogashira cross-coupling with DTP-BT-X chromophores. **b.** Synthesis of three iodine functionalized DTP-BT derivatives: (i) *n*-BuLi, Me$_3$SnCl, THF; (ii) Pd$_2$(dba)$_3$, P(*o*-tolyl)$_3$, toluene, DMF; (iii) NIS, CHCl$_3$, AcOH; (iv) malononitrile, piperidine, CHCl$_3$.

3.1 Chromophore synthesis

Three different push-pull type chromophores were synthesized by changing the substituents on the electron-deficient benzothiadiazole (BT) acceptor unit from a hydrogen atom to an aldehyde or a dicyanovinyl group, as shown in **Scheme 1 b**. These donor-acceptor chromophores were selected because of their envisaged charge separation after excitation, easy tuning of the optical properties through the introduction of various substituents and compact size, which enables a high diamond surface coverage. In previous work we functionalized iodophenyl terminated diamond thin films with alkyne functionalized dithieno[3,2-*b*:2',3'-*d*]pyrrole-2,1,3-benzothiadiazole (DTP-BT) molecules via Sonogashira cross-coupling.[33] By using the same chromophore system, the influence of the initial surface functionalization strategy (iodophenyl vs. ethynylphenyl or multilayer vs. monolayer) on the photocurrent generation of the resulting photoelectrodes can be directly compared. The dithienopyrrole (DTP) donor unit (**1**) was synthesized in two steps starting from 3-bromothiophene, as described previously.[33] After monostannylation using *n*-butyl lithium and trimethylstannylchloride, a Stille cross-coupling was performed with 4-bromo-2,1,3-benzothiadiazole (**2**). The resulting chromophore, DTP-BT (**3**), was then prepared for immobilization on the diamond surface via Sonogashira cross-coupling through introduction of an iodine functionality with *N*-iodosuccinimide (NIS). The two other chromophores, **7** and **8**, were prepared in a similar fashion. However, instead of acceptor unit **2**, 7-bromo-2,1,3-benzothiadiazole-4-carbaldehyde (**5**)[49, 50] was employed during the Stille cross-coupling. The dithieno[3,2-*b*:2',3'-*d*]pyrrole-2,1,3-benzothiadiazole-4-carbaldehyde (DTP-BT-CHO, **6**) compound was also iodinated, resulting in the second dye (**7**). Finally, the dicyanovinyl derivative, I-DTP-BT-DCV (**8**), was prepared through a Knoevenagel condensation with malononitrile.

The optical and electrochemical properties of the three chromophores were investigated by UV-Vis absorption spectroscopy and cyclic voltammetry, respectively (**Table 1**). The complete UV-Vis absorption spectra of the designed chromophores (**Figure 1 a**) indicate that stronger electron-withdrawing properties of the acceptor part result in a decrease of the optical gap and hence a red shift of the absorption maximum (λ_{max}). DTP-BT (**4**) shows a λ_{max} for the intramolecular charge transfer band at 474 nm and a moderate molar extinction coefficient (ε) of 18 600 M^{-1} cm^{-1}. By exchanging the hydrogen end group by an aldehyde in chromophore **7**, the absorption maximum is red-shifted to 533 nm and ε increases to 22 000 M^{-1} cm^{-1}. For DTP-BT-DCV (**8**), which contains the strongest electron-withdrawing dicyanovinyl group, λ_{max} is shifted further to the red part of the spectrum with a λ_{max} of 608 nm and a molar extinction coefficient that is almost twice as large as for DTP-BT (ε = 30 800 M^{-1} cm^{-1}).

Table 1 | Overview of the experimentally obtained optical and electrochemical data of the DTP-BT, DTP-BT-CHO and DTP-BT-DCV chromophores.

Dye	λ_{max} (nm)	ε (M^{-1} cm^{-1})	E_{ox} (eV)	E_{red} (eV)	E_{HOMO} (eV)	E_{LUMO} (eV)	ΔE_{opt} (eV)	ΔE_{EC} (eV)
DTP-BT	474	18 600	0.43	-1.49	-5.21	-3.29	2.30	1.92
DTP-BT-CHO	533	22 000	0.68	-1.16	-5.46	-3.62	2.04	1.84
DTP-BT-DCV	608	30 800	0.69	-0.84	-5.47	-3.94	1.80	1.53

E_{ox} and E_{red} represent the oxidation and reduction potential of the chromophores, whereas the optical gap as determined by UV-Vis is given by ΔE_{opt} and the electrochemically calculated gap is given by ΔE_{EC}

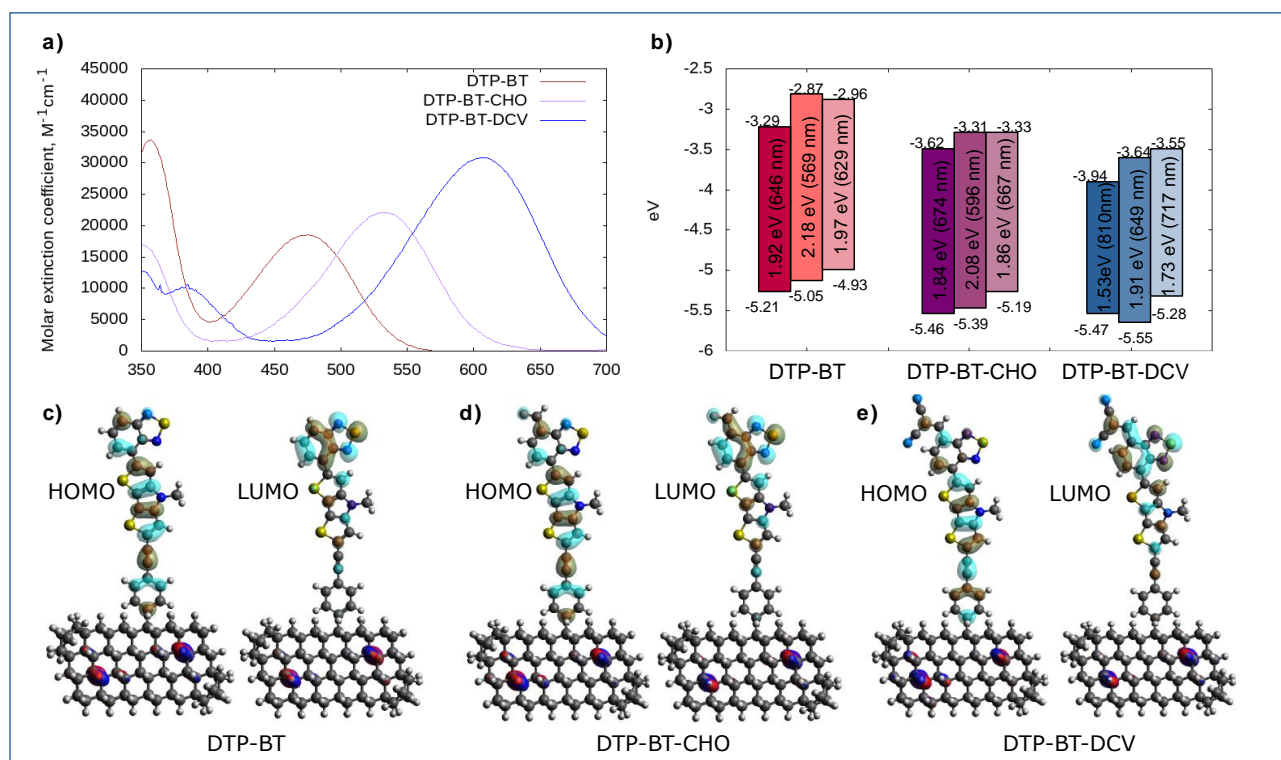**Figure 1 | a.** Experimental UV-Vis absorption spectra of DTP-BT, DTP-BT-CHO, and DTP-BT-DCV chromophores. **b.** Highest occupied molecular orbital (HOMO) and lowest unoccupied molecular orbital (LUMO) energy levels and corresponding band gap of the individual chromophores (in eV). For each dye molecule the experimental data is represented by the left-most box, the calculated energy levels are provided by the middle box and the right-most box includes the effect on the HOMO/LUMO levels when the chromophores are grafted onto the diamond surface. **c-e**. Arrangement of the chromophores grafted on B-doped diamond as obtained by DFT computing. Blue and red surfaces are the frontier orbitals of the whole system located on B atoms. Cyan and brown colors highlight frontier orbitals of the molecules.

In **Figure 1 b** the experimentally determined highest occupied molecular orbital (HOMO) and lowest unoccupied molecule orbital (LUMO) energy levels of the different chromophores are represented by the left-most box (darkest color). It is known that structural changes to the acceptor unit have the largest influence on the location of the LUMO energy level.[59] Hence, the strong decrease of the LUMO level, from -3.29 to -3.62 and -3.94 eV for the DTP-BT, DTP-BT-CHO and DTP-BT-DCV series, is in line with our

expectations. The decrease in the HOMO level was, accordingly, much less pronounced (from -5.21 to -5.46 and -5.47 eV). Note however, that these measurements were performed for standalone chromophores and not on the diamond-chromophore complex. In order to obtain a better insight into the electron configuration and function of this hybrid system, the HOMO and LUMO levels of the chromophores that are immobilized on the diamond surface were determined theoretically by DFT calculations. These value are given by the right-most box in **Figure 1 b** (lightest color) and for the theoretical computing, a finite hydrogenated diamond (111) slab was designed including 448 carbon atoms and 4 boron atoms. The concentration of boron in these slabs corresponds approximately with the employed B:NCD substrates, and the chosen size was proven to be big enough to model an infinite slab of diamond.[60] In the case of these diamond-chromophore complexes a similar trend was observed for their HOMO/LUMO levels with regards to the standalone chromophores. However, after grafting of the chromophores on diamond it is obvious that both the HOMO and LUMO energy is shifted by approximately 0.3 eV. This may be due to enlargement of the conjugated chain after the linker addition and grafting to diamond. To ensure fast hole injection from the HOMO of the dye into diamond, the HOMO energy level should be situated below the valence band maximum (VBM) of diamond, which is located at *ca*. -5.50 eV in contact with an electrolyte solution.[61] In all cases, the HOMO level is located below the VBM of diamond, however, through the application of an external voltage, this difference can be overcome. Conversely, all LUMO levels lie well above that of methyl viologen (MV^{2+}) (-4.22 eV), which is employed as a redox electrolyte. Electrons could be thus easily transferred from the molecule to the electrolyte after excitation with light. From all chromophores, we expect that DTP-BT-DCV is the most suitable for diamond photosensitization, due to a more favorable location of its HOMO energy level with respect to the diamond VBM and the strong absorption over a broad range.

This assertion is also supported by the molecular orbital localization on an atomic scale. **Figure 1 c-e** shows the arrangement of the chromophores grafted on boron-doped diamond as obtained by DFT computing. Blue and red surfaces are the frontier orbitals of the whole system located on B atoms. Cyan and brown colors highlight frontier orbitals of the molecules. One can see that all three chromophores are grafted in the same upright arrangement on diamond. No difference in bending, rotation, inclination is observed. Thus, no structural effect on charge transfer between the molecules and diamond is expected. The depicted molecular orbitals show that the HOMO of the chromophores is delocalized along the entire conjugated system including the link to diamond, while the LUMO is centered in the BT moiety. The spatial separation of HOMO and LUMO seems the most pronounced in the case of the DTP-BT-DCV chromophore. This finding supports the idea of exciton dissociation and charge transfer, as an eventual optical transition centered on the chromophores from the HOMO to the LUMO might lead to charge separation in which the electron goes to the benzothiadiazole moiety, in agreement with its expected electron acceptor properties. Therefore, we have performed further computational analysis of the excited states and related charge transitions. The computed UV-Vis spectra are shown in the supporting information (**Figure S1**) and they reveal a strong interaction between the chromophores and the diamond. After grafting of the chromophores on diamond the first intense absorption band is red-shifted

and split into several peaks. Key data obtained from the analysis of these split excited states is summarized in **Table 2**. For the DTP-BT molecule, two major excitations, α and β, were observed and they transfer 0.15 and 0.16 electrons from diamond to the benzothiadiazole unit, respectively, resulting in an electron-hole couple that is separated by 3-4 Å. After addition of the formyl group for DTP-BT-CHO, two similar excitations were observed. One of these transitions has an increased oscillator strength (0.73) and is capable of transferring 0.18 electrons across a distance of 4.61 Å. Finally, DTP-BT-DCV shows two strong signals with an oscillator strength of 0.57 and 0.60 that transfer 0.18 and 0.19 electrons to the acceptor unit, respectively. This is more than any other excitation on the previous molecules. Moreover, a third excitation, γ, was observed, which is capable of transferring 0.75 electrons despite its weaker oscillator strength of 0.12. Thereby it creates an electron-hole couple that is separated by 19.94 Å with an exciton binding energy as low as 0.74 eV. The strong charge separation effect of the γ excitation on the DTP-BT-DCV molecule is clearly evidenced in **Figure S2**, where holes and electrons are strongly separated. The DFT based calculations thus show that among the investigated molecules, DTP-BT-DCV should also provide the most efficient photo-generated charge separation and injection to diamond.

Table 2 | Analysis of the excited states for the chromophores grafted on boron-doped diamond.

Dye	Excitation	E (eV)	Osc. Str.	Q	Δr (Å)	E_B (eV)
DTP-BT	α	1.82	0.30	0.15	3.11	1.30
	β	1.83	0.30	0.16	3.65	1.37
DTP-BT-CHO	α	1.82	0.73	0.18	4.61	1.34
	β	1.83	0.32	0.11	2.55	1.34
DTP-BT-DCV	α	1.75	0.57	0.18	3.26	1.30
	β	1.75	0.50	0.19	3.47	1.29
	γ	1.78	0.12	0.75	19.94	0.74

These excited states were obtained due to splitting of the first optically active excited state of the standalone chromophore after splitting. For each molecule, each transition is denoted with the letters of the Greek alphabet. Only the transitions with the oscillator strength > 0.10 and high charge transfer were analyzed. Q is an effective electron charge transferred between the benzothiadiazole to the diamond (positive sign = electrons transferred to BT). Charge transfer distance is denoted as Δr. E_B stands for the exciton binding energy.

3.2   Primary surface functionalization: Diazonium grafting

The envisaged monolayer functionalization of B:NCD with the various DTP-BT-X chromophores (where X is either a hydrogen, aldehyde or dicyanovinyl group; **Scheme 1**) was realized through the electrochemical diazonium grafting of TMS-protected ethynylbenzenediazonium tetrafluoroborate, as described by Natsui *et al.* as shown in **Figure 2 a**.[62] Diazonium grafting was performed electrochemically by employing a freshly H-terminated diamond film as the working electrode in a cyclic voltammetry setup. The electrode was submerged in a solution of the diazonium salt (5 mM) and tetrabutylammonium hexafluorophosphate (0.1 M) in acetonitrile. The potential was cycled between +600 and -750 mV (*vs.* a Ag/AgCl reference electrode) at a scan rate of 50 mV s^{-1}. In this way, electrons are ejected from diamond into the solution, which results in a reduction of the diazonium salt to the corresponding radical and its immediate grafting on the surface.[29] During the first scan, a sharp

reduction peak was observed in the cyclic voltammogram at -335 mV, as shown in **Figure 2 b**. In the subsequent scans, this reduction peak strongly decreased, indicating that after one cycle a near complete passivation of the diamond surface with TMS protected ethynylphenyl molecules was obtained. The cathodic current for the reduction peak in the first scan is approximately 4 times lower than the one for electrochemical grafting of *in situ* diazotized 4-iodoaniline.[33] Since the amount of generated radicals and, thus, the thickness of the grafted layer is directly related to the charge that is passed through the system, this hints already at the formation of thinner layers.[63]

After electrochemical diazonium grafting, the TMS protective groups were removed by stirring the functionalized diamond samples in a 5 mL THF solution containing 100 mM tetrabutylammonium fluoride (TBAF). Both the grafting and the deprotection step were analyzed via cyclic voltammetry in an acetonitrile electrolyte solution containing 1 mM ferrocene and 100 mM TBAF. Cyclic voltammograms for H-terminated (B:NCD-H, black curve), TMS protected (B:NCD-Ph-Eth-TMS, blue curve) and alkyne functionalized (B:NCD-Ph-Eth, red curve) diamond surfaces were recorded between -250 and +1000 mV at a scan rate of 50 mV s^{-1} (**Figure 2 c**). For the H-terminated B:NCD electrode, the voltammogram demonstrated two narrow peaks that correspond with the oxidation and reduction of ferrocene. The peak separation potential (ΔE_p) of 70 mV is in line with values that are typically obtained for polycrystalline H-terminated diamond.[64] After electrochemical grafting of the TMS protected diazonium salt, the peak separation value increased to ΔE_p = 108 mV, accompanied with a decrease of both the oxidation and reduction peak currents. These changes in electrochemical behavior suggest that the "bulky" TMS groups impede efficient electron transport between ferrocene and the diamond electrode, thus acting as a barrier for electric charge transfer.[65] Yet, immediately after treatment with TBAF, the peak separation potential and currents are restored to the values as obtained for H-terminated diamond, which suggests successful deprotection leading to an alkyne functionalized surface.

The successful functionalization of the H-terminated diamond electrodes was confirmed by analysis of the surface composition via X-ray photoelectron spectroscopy (XPS). Indeed, after electrochemical diazonium grafting, two new signals were detected at 151.5 and 100.5 eV, which correspond to the Si 2s and Si 2p peaks, respectively. Calculation of the relative atomic surface concentration from XPS high resolution spectra revealed the presence of 2.3 ± 0.5 at.% Si (measured over two samples at two different locations, area = 0.7 × 0.3 mm^2). The high resolution Si 2p peak (**Figure 2 d**) was deconvoluted into three contributions: Si-C at 100.6 eV (79.5%), Si-N at 101.7 eV (18.2%) and Si-O at 102.4 eV (2.3%).[66] As expected, the majority of the Si 2p peak is composed of Si-C bonds that arise from the TMS protective groups. Remarkably, there is also a significant contribution from Si-N bonds. XPS analysis showed that there is about 1.8 ± 0.26 at.% of nitrogen on the sample surface. A possible explanation for this observation is that N$_2$ is adsorbed onto the surface by storing the diamond samples under nitrogen atmosphere or drying them under a nitrogen stream after functionalization and rinsing. It is worth to mention that the observed nitrogen should not originate from azo-bridges because the bulky TMS groups shield the *ortho* positions from multilayer formation.[67] After deprotection of the TMS groups with TBAF,

the surface Si concentration reduced to 0.15 ± 0.06 at.%, which translates to a reaction efficiency of 94%.
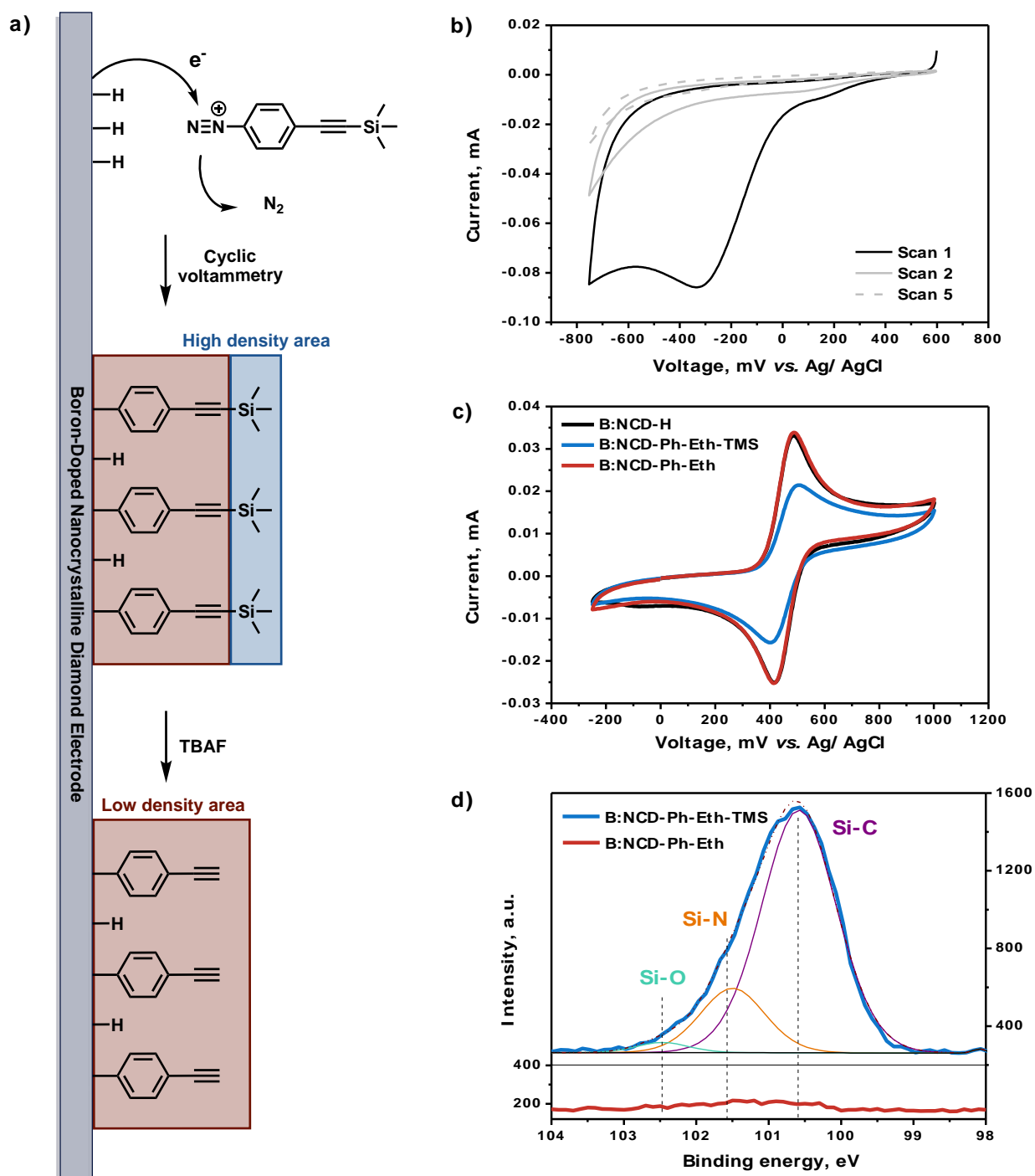

Figure 2 | a. Preparation of an ethynylphenyl functionalized B:NCD surface. **b.** Cyclic voltammograms for the electrochemical grafting of 4-(trimethylsilyl) ethynylbenzenediazonium tetrafluoroborate. **c.** Cyclic voltammograms for H-terminated (black), TMS protected (blue) and alkyne functionalized (red) B:NCD electrodes in a 1 mM ferrocene solution in acetonitrile. **d.** Deconvoluted Si 2p high resolution XPS spectra of TMS protected B:NCD (blue) and the Si 2p peak shape of alkyne functionalized B:NCD (red).

Additional information on the primary surface functionalization via electrochemical diazonium grafting and the subsequent deprotection of the TMS groups can be obtained from the C 1s peak at 283.8 eV, which is further explained in the supplementary information (**Figure S3**). XPS analysis was also employed to estimate the density of the functionalized layer and its structural organization, which allows for the differentiation between monolayer and multilayer functionalization.[45] The density of the obtained layer after diazonium grafting can be assessed by comparing the relative atomic concentrations of boron after grafting and after deprotection of the TMS groups. The boron concentration after diazonium grafting was about 1.67 ± 0.06 at.%, whereas after deprotection of the TMS groups with TBAF the boron content increased to 2.68 ± 0.22 at.%. Since the TMS group has a thickness, which is les than 3 Å,[47] this difference in boron concentration cannot be attributed to merely a change in penetration depth of the X-rays. We suppose that the observed change in boron content has to be related to a change in efficiency of the functional surface layer to scatter the electrons from boron atoms from the diamond "bulk".[47] Hence, it can be assumed that the density of the grafted layer is determined by the packing density of the TMS groups rather than that of the benzene molecules since the electrons from boron atoms are scattered more efficiently before the deprotection step, which results in a lower boron at.%. As a result, the ethynylphenyl molecules are likely not packed very densely and gaps are present in between the different molecules, as shown in **Figure 2**. This observation is in line with the work by Hapiot *et al*., who tuned the density of the functionalized surface by changing the protective group from trimethylsilyl (TMS) to triethylsilyl (TES) and triisopropyl (TIPS) moieties.[48]

By employing angular resolved XPS (ARXPS), the organization of the surface layer could be determined. In a randomly oriented film, which is associated with multilayer formation, the electrons from the Si and C atoms have more or less equal trajectories through the functionalized film and undergo equal amounts of scattering (**Figure 3 a**).[45] In a proper monolayer, however, all Si atoms are organized at the topmost part of the functionalized layer. Therefore, when increasing the angle under which the samples are measured, an increase of the Si/C ratio might be expected (**Figure 3 b, c**). However, it should be mentioned that we are not dealing with bare Si atoms, but $Si(CH_3)_3$ groups, where the methyl groups determine the density of the layer. Hence, rather than an increase of the Si/C ratio, a decrease thereof is expected due to the presence of these methyl groups at the topmost surface in case of a well-organized layer. This hypothesis is rationalized by the fact that for the TMS protected surfaces, the $C-H_X$ component of the C 1s peak has the strongest contribution (**Figure S3** and **Table S1**). ARXPS measurements were performed at six different substrate angles θ and the results are shown in **Figure 3 c**.
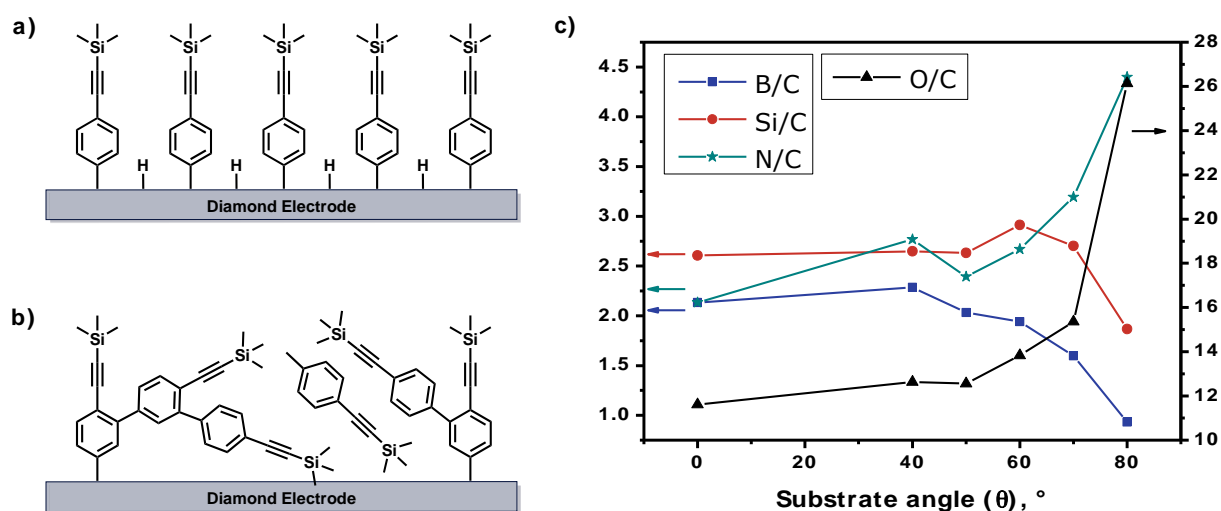
Figure 3 | a. Schematic representation of a well-organized monolayer of TMS protected ethynylphenyl molecules. **b.** Schematic representation of a randomly organized TMS protected ethynylphenyl layer corresponding with multilayer functionalization. **c.** B/C (blue), Si/C (red), N/C (green) and O/C (black) ratios of their respective atomic concentrations for angular resolved XPS measurements at substrate angles (θ) of 0, 40, 50, 60, 70 and 80° after electrochemical diazonium grafting of TEBDT.

The B/C ratio remained more or less constant until the substrate was tilted at angles higher than 40°, after which it started to decrease to a value of 0.9 at 80°. This indicates that with increasing substrate angles, higher volumes of the actual surface are being measured in comparison with the diamond bulk. As hypothesized, the Si/C ratio also declined with increasing contact angles. This decrease, however, only starts at angles > 60°, which can be explained by the fact that only at sufficiently high angles, there is enough difference in the measured volume of the methyl groups and the Si atoms, which are both located at the interface between the functionalized layer and the atmosphere. The N/C and O/C ratios, however, demonstrate a rather exponential increase with increasing θ values. This suggests that both nitrogen and oxygen species are adsorbed onto the surface rather than that they are integrated in the grafted layer (*e.g.* through the formation of azo-bridges in case of nitrogen).

Based on these results we assume that the electrochemical diazonium grafting of TEBDT on B:NCD also results in monolayers, which has only been proven for flat surfaces such as pyrolized photoresist films and glassy carbon until now.[47, 48, 58] AFM scratching experiments were performed as well, but due to the high roughness of the nanocrystalline diamond films, no clear conclusions could be drawn from those results.

3.3 Secondary surface functionalization: Sonogashira cross-coupling

With regards to the development of BDD electrodes for photoelectrochemical applications, and ultimately the development of p-type DSSCs, two parameters are of utmost importance, *i.e.* a high surface coverage with chromophores and minimal surface contamination. The latter can result in charge trapping of the photogenerated holes and electrons. Charge transport also plays an important role. In this respect,

fully conjugated systems are desired for the fabrication of photoelectrodes. In contrast to the Stille cross-coupling, it has been shown that both the Suzuki and Sonogashira cross-coupling, as well as the Cu(I) catalyzed azide-alkyne cycloaddition (CuAAC), yield decent surface coverages without severe surface contamination.[31, 38, 68] In previous work we demonstrated that BDD films functionalized via Sonogashira cross-coupling afforded photocurrents that are three times higher than when CuAAC chemistry was employed.[33] Hence, in this work the Sonogashira cross-coupling was applied to immobilize the DTP-BT, DTP-BT-CHO and DTP-BT-DCV chromophores onto diamond electrodes functionalized with alkyne monolayers, as illustrated in **Scheme 2**.
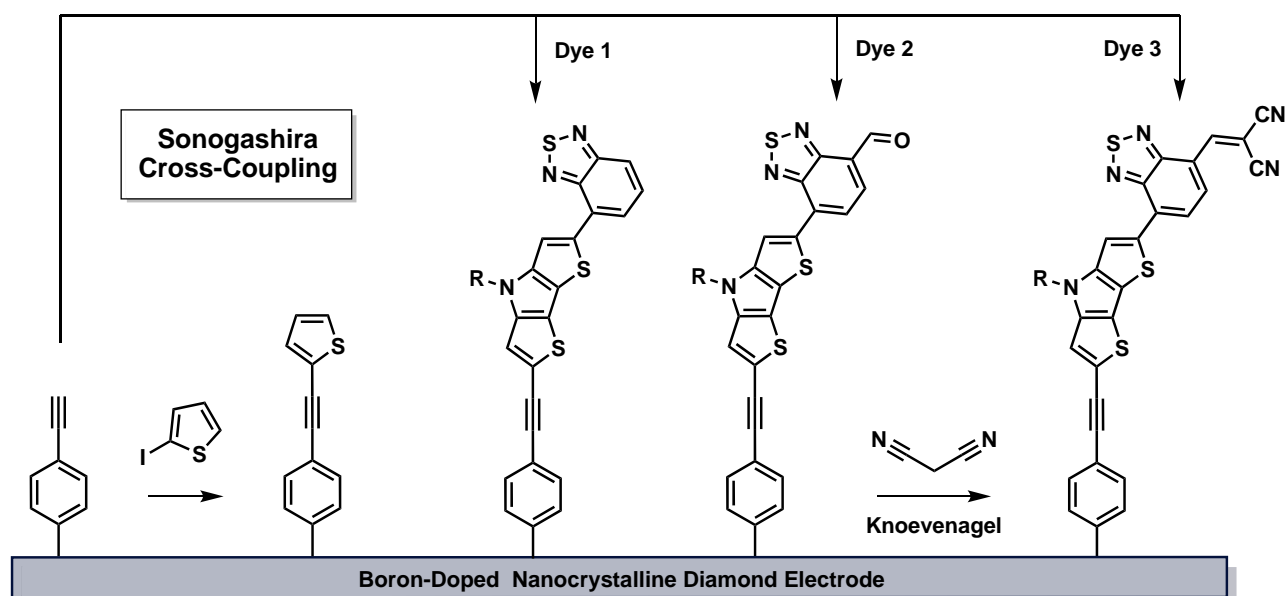
Scheme 2 | Sonogashira cross-coupling of 2-iodothiophene, I-DTP-BT (dye 1), I-DTP-BT-CHO (dye 2) and I-DTP-BT-DCV (dye 3) on B:NCD electrodes functionalized with a monolayer of ethynylphenyl molecules.

Before employing the actual chromophores, a simple proof of concept reaction was performed with commercial 2-iodothiophene, using Pd(PPh$_3$)$_2$Cl$_2$ (5 mol%) and CuI (10 mol%) in a solvent mixture (3:1) of THF and diisopropylamine (DIPA). After thorough rinsing and sonication in various solvents, and the use of a solution of ammonium diethyldithiocarbamate in THF to remove any physisorbed Pd or Cu that might have remained after the Sonogashira cross-coupling, the surface composition was analyzed by means of XPS. The relative atomic concentration of S was about 0.35 ± 0.07 at.%. The sulfur content can be used to estimate the surface coverage since it can only originate from the coupled thiophene molecules. The observed S concentration is *ca.* 6 times lower than the values obtained before for the inverted reaction, wherein 2-ethynylthiophene is coupled to iodophenyl functionalized B:NCD electrodes.[38] Yet, it is not possible to make clear-cut conclusions on the degree of functionalization for the "normal" and "inverted" Sonogashira cross-coupling reaction since in the current experiment the ethynylphenyl layers are much thinner. Hence, a higher content of carbon atoms from the diamond bulk is measured by XPS, resulting in a lower relative atomic S concentration.

The functionalization of the ethynylphenyl decorated diamond electrodes with push-pull type dyes was then optimized for the iodine-functionalized DTP-BT chromophore **4** (dye 1), since this has the lowest synthetic complexity. An overview of the employed reaction conditions and resulting XPS analyses of the surfaces, which gives us an idea on the degree of functionalization and possible contamination, is presented in **Table 3**. Various Pd-ligand catalyst systems were evaluated, while the amount of dye was kept constant at 50 µmol in a 3:1 mixture of THF and DIPA. The catalytic systems increase in reactivity in the following order: $Pd(PPh_3)_2Cl_2$ < Pd_2dba_3 + $P(o\text{-tolyl})_3$ < $Pd(OAc)_2$ + SPhos/XPhos. The first two catalytic systems have a moderate reactivity and are commonly employed for the synthesis of conjugated small molecules or polymers via Pd catalyzed cross-coupling reactions in solution.[69] The last system, on the other hand, comprises $Pd(OAc)_2$ and either one of the two highly reactive ligands SPhos or XPhos, previously employed for diamond surface functionalization via Suzuki cross-coupling.[30] These monodentate biarylphosphine ligands have been developed by the Buchwald group and facilitate the oxidative addition step due to their electron rich nature. Since they are rather sterically demanding, only a 12-electron Pd complex will be formed, which also increases the reaction rate of the reductive elimination, allowing for faster cross-coupling reactions.[70, 71]

Table 3 | Analysis of the surface composition by means of XPS for BDD functionalization with I-DTP-BT chromophore **4** (dye 1) via Sonogashira cross-coupling.

Entry	Catalyst/Ligand	Dye	C at.%	O at.%	N at.%	B at.%	S at.%	Pd at.%	Cu at.%
1₁	$Pd(PPh_3)_2Cl_2$ (5 mol%)	1	89.2	7.8	2.4	-	0.5	-	-
1₂		(50 µmol)	88.1	7.2	1.9	2.4	0.4	-	-
2₁	Pd_2dba_3 (3 mol%) /	1	87.4	7.5	2.2	2.3	0.6	-	-
2₂	$P(o\text{-tolyl})_3$ (12 mol%)	(50 µmol)	87.9	7.5	1.7	2.4	0.5	-	-
3₁	$Pd(OAc)_2$ (6 mol%) /	1	87.4	7.6	2.2	2.3	0.5	-	-
3₂	XPhos (6 mol%)	(50 µmol)	87.4	7.9	1.8	2.5	0.4	-	-
4₁	$Pd(OAc)_2$ (6 mol%) /	1	87.6	7.5	2.1	2.3	0.5	-	-
4₂	XPhos (6 mol%)	(50 µmol)	87.6	7.4	2.4	2.1	0.5	-	-
5	- (control experiment)	1 (50 µmol)	88.6	7.2	1.1	3.0	0.1	-	-

General reaction conditions: CuI (10 mol%), dry THF (3 mL), diisopropylamine (1 mL), 60 °C, 18 h. Each sample was measured at two different locations (0.7 × 0.3 mm^2), which is indicated by the subscripts in the entry column. Only traces of Pd and Cu were detected (≤0.05 at.%).

Looking at the relative atomic concentrations for S in **Table 3**, we can conclude that the degree of functionalization is independent of the employed catalyst system. All samples were analyzed by XPS at two different locations and surface contamination with Pd or Cu was always less than 0.05%. The absence of surface impurities is attributed to the application of a Pd scavenger, ammonium diethyldithiocarbamate, which is soluble in organic solvents.[72] Since the chromophores are also easily solubilized in organic solvents like THF, toluene or chloroform, any trapped transition metals are removed more efficiently than with the water-soluble sodium diethyldithiocarbamate employed before. The

average S concentration (taken over all four samples) after Sonogashira cross-coupling was determined to be 0.49 ± 0.064 at.%. In comparison with the S concentration for the inverted Sonogashira cross-coupling of alkyne functionalized DTP-BT on iodophenyl terminated diamond (S content of 2.4 at.%), this value is again *ca*. 5 times lower, which is similar to the results obtained for the thiophene model compound.[33] The N concentration after Sonogashira cross-coupling increased from an average value of 1.6 ± 0.14 at.% (for B:NCD-Ph-Eth) to 2.08 ± 0.26 at.% (for B:NCD-Ph-Eth-DTP-BT). This increase of 0.48 at.% is identical to the increase of the S concentration and corresponds perfectly to the 1:1 ratio of nitrogen and sulfur atoms in the chromophore. A control experiment without addition of a Pd catalyst system was also performed to determine whether the obtained results are due to an actual cross-coupling reaction or mere adsorption on the surface. In this case, only very low S concentrations (0.1 at.% S) were detected, likely attributable to small amounts of physisorbed molecules. Hence, we can conclude that the dye molecules are covalently immobilized onto the surface of the functionalized diamond electrodes upon applying Sonogashira cross-coupling reactions. The changes on the diamond surface during the three-step functionalization protocol are visualized in an overlay of the XPS survey spectra at different stages (**Figure S4**).

The covalent attachment of the two other chromophores, *i.e.* DTP-BT-CHO (dye 2) and DTP-BT-DCV (dye 3), onto BDD was performed with Pd_2dba_3 as a catalyst and P(*o*-tolyl)$_3$ as the ligand, since this system resulted in the highest surface coverage (even though the difference is not very significant). The exact reaction conditions are given in **Table S2** and every sample was analyzed at three locations to estimate the homogeneity. The relative atomic concentration of S slightly increased (in comparison with dye 1) for immobilization of the DTP-BT-CHO chromophore, up to a value of 0.73 ± 0.058 at.%. This increased degree of functionalization might be related to an improved oxidative addition rate of the Pd complex during the cross-coupling reaction due to the additional electron-deficient aldehyde group (although the aldehyde is small). The N concentration after Sonogashira cross-coupling was about 2.27 ± 0.058 at.%, which is an increase of 0.67 at.%. This value is again in good agreement with the 1:1 ratio of S:N in the chromophore system. During functionalization of the diamond electrodes with dye 3 (DTP-BT-DCV), however, an unexpected change in color of the reaction solution from blue to purple was observed almost instantaneously. Matrix-assisted laser desorption/ionization time-of-flight (MALDI-ToF) mass analysis of the reaction mixture revealed that the dicyanovinyl group is susceptible to a nucleophilic attack by DIPA, which results in degradation of the chromophore, as shown in **Figure S5** and **S6**. By employing a non-nucleophilic such as Cs_2CO_3, no degradation occurred and DTP-BT-DCV could be successfully attached onto the surface (**Table S2,** entry 8). The sulfur coverage (1.03 ± 0.23 at.%) was again somewhat higher, which could be attributed to the even stronger electron-withdrawing properties of the dicyanovinyl-substituted BT group. Another route toward obtaining DTP-BT-DCV functionalized surfaces was explored by transforming the aldehyde group of a DTP-BT-CHO functionalized diamond electrode into the corresponding dicyanovinyl group through a Knoevenagel condensation with malononitrile (**Table S2**, entry 9). As expected, the S concentration was comparable with that for dye 2 (0.63 ± 0.058 at.%), but a significant increase in N concentration was observed (3.00 ± 0.17 at.%). This corresponds with a S:N

ratio of 3:6.6, which is somewhat higher than the expected 3:5 ratio. Nevertheless, based on this increased N concentration, we can confirm transformation of the surface aldehyde groups to dicyanovinyl moieties. In **Figure 4**, the XPS survey spectra upon functionalization with dyes 1, 2 and 3 are shown, together with the deconvoluted high resolution S 2p peaks. For further photoelectrochemical analysis, the B:NCD-Ph-Eth-DTP-BT-DCV samples obtained via Sonogashira cross-coupling using Cs_2CO_3 as a base have been employed, since this approach resulted in the highest surface coverage.
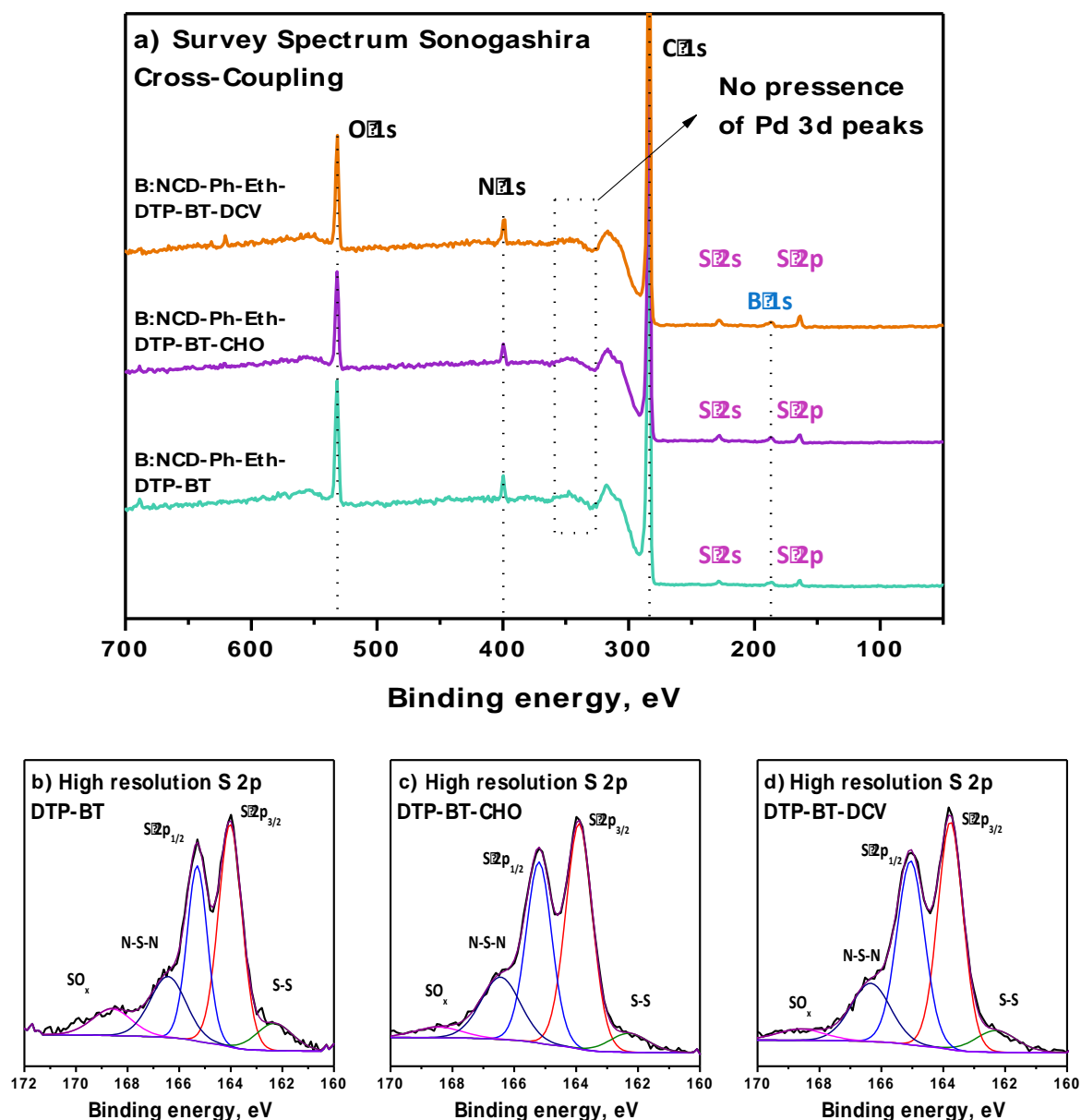
Figure 4 | a. Overlay of the XPS spectra for B:NCD electrodes functionalized with DTP-BT (cyan curve), DTP-BT-CHO (purple curve) and DTP-BT-DCV (orange curve) via Sonogashira cross-coupling. **b/c.** Deconvoluted high resolution S 2p peak for DTP-BT-CHO and DTP-BT-DCV functionalized diamond electrodes, respectively.

3.4 Photoelectrochemistry and photovoltage measurements

Photoelectrochemical measurements were finally performed to investigate the influence of monolayer functionalization with the different chromophores. During these measurements, functionalized diamond electrodes were employed as the working electrode in a typical three-electrode voltammetry set-up. The samples were irradiated using white light with an intensity of 1 sun in an aqueous electrolyte solution of methyl viologen (MV^{2+}), which serves as the redox electrolyte and transports photo-excited electrons to the counter electrode. The electrodes were first equilibrated in a dark environment before illuminating them for intervals of approximately 10 seconds, as shown in **Figure 5 a**. Application of a negative voltage has previously been demonstrated to positively influence the cathodic photocurrents due to the generation of a net vectorial flow of electrons from the photocathode to the counter electrode through the redox electrolyte.[73, 74] Accordingly, a negative bias of -0.2 V was applied during the chronoamperometric measurements.
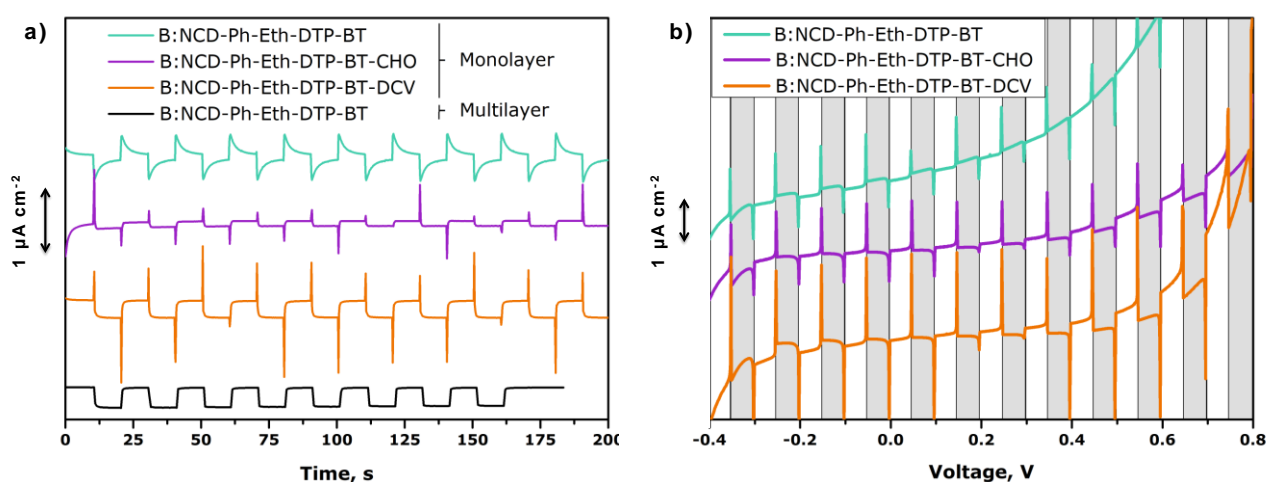

Figure 5 | a. Photocurrent densities and **b.** chopped light polarization curves for B:NCD electrodes functionalized with the three types of DTP-BT-X chromophores in a 5 mM methyl viologen solution (in 0.1 M Na_2SO_4) under white light illumination (100 mW cm^{-2}; simulated 1.5G solar spectrum). For the photocurrent densities 10 s 1:1 dark light/intervals were applied at bias of -0.2 V. The black curve for a multilayer functionalized surface was reproduced from previous work.[33] For the chopped light polarization curves the applied bias was changed from +0.8 to -0.4 V. In the shaded areas, the samples were not illuminated.

The chronoamperometric measurements for the B:NCD electrodes functionalized with DTP-BT (cyan curve), DTP-BT-CHO (purple curve) and DTP-BT-DCV (orange curve) all demonstrated a strong decrease of the initial photocurrent after illuminating the samples with white light. For the B:NCD-Ph-Eth-DTP-BT electrodes, this decrease occurred relatively slowly, whereas for the other two materials a much faster decrease of the currents was observed. The observed behavior is probably related to undesired charge recombination and is likely a direct result of the employed monolayer functionalization strategy.[40] Multiple control experiments were performed to rule out any influence from the measurement set-up or

potential damaging of the surface caused by X-ray irradiation during the XPS measurements. Also, identical highly doped diamond electrodes on p-type Si, as previously employed for the functionalization with DTP-BT chromophores (black curve) via the inverted strategy, were used in this study.[33] Hence, the main difference between this work and our previous report is the initial surface functionalization strategy. Through XPS analysis of the BDD electrodes decorated with TMS protected ethynylphenyl molecules, it was already demonstrated that the density of the layer is determined rather by the bulky protecting groups and not the phenyl linkers. We expect that gaps in between the grafted molecules provide a pathway for recombination of the photogenerated electrons. This hypothesis is supported by the information obtained from the chopped-light polarization curves for all three types of functionalized photocathodes, as shown in **Figure 5 b**. These curves demonstrate relatively large anodic photocurrents (n-type behavior) upon illumination when an external bias between +0.3 and +0.8 V is applied. Moreover, cathodic photocurrents (p-type behavior) are only obtained when the bias is equal or lower than 0.0 V. Although anodic photocurrents have been reported previously for sensitized BDD electrodes,[33, 39] our values are exceptionally high and the transition to cathodic photocurrents requires remarkably low potentials. This indicates that the functionalized diamond electrodes rather behave as photoanodes than photocathodes and that after excitation electrons are injected into diamond. In case of electrodes functionalized via the multilayer approach, this pathway is less accessible since there is a more dense and thicker network of phenyl molecules that potentially serves as an electron-blocking layer. To circumvent this issue for a monolayer functionalization the electron blocking properties of B:NCD would need to be improved, e.g. by additional surface passivation in between the chromophore molecules using various surface chemical groups of diamond (oxygen-related moieties) or some other small molecules.

The mechanism for recombination can be that either the electrons are directly injected from the chromophore into diamond or they are first transferred to the methyl viologen electrolyte before recombination occurs. By employing scanning Kelvin probe (SKP) microscopy, the surface potential can be determined in dark and under illumination, providing information on the behavior of the generated charges in the absence of an electrolyte solution. For DTP-BT, DTP-BT-CHO and DTP-BT-DCV functionalized diamond electrodes, the surface potential decreased to a value of 35 mV, 64 mV and 68 mV, respectively, as shown in **Figure 6 a**. This indicates that after photoexcitation, the generated holes are successfully injected into BDD, while the electrons remain at the interface. Therefore, we can assume that in the presence of a MV^{2+} electrolyte solution, the electrons are at first transferred to the redox electrolyte, which seems plausible since its redox potential lies well below the LUMO energy level in all cases. Afterwards the electrolyte is reoxidized at the BDD electrode instead of the counter electrode, leading to the observed charge recombination (as schematically shown in **Figure 6 b**).
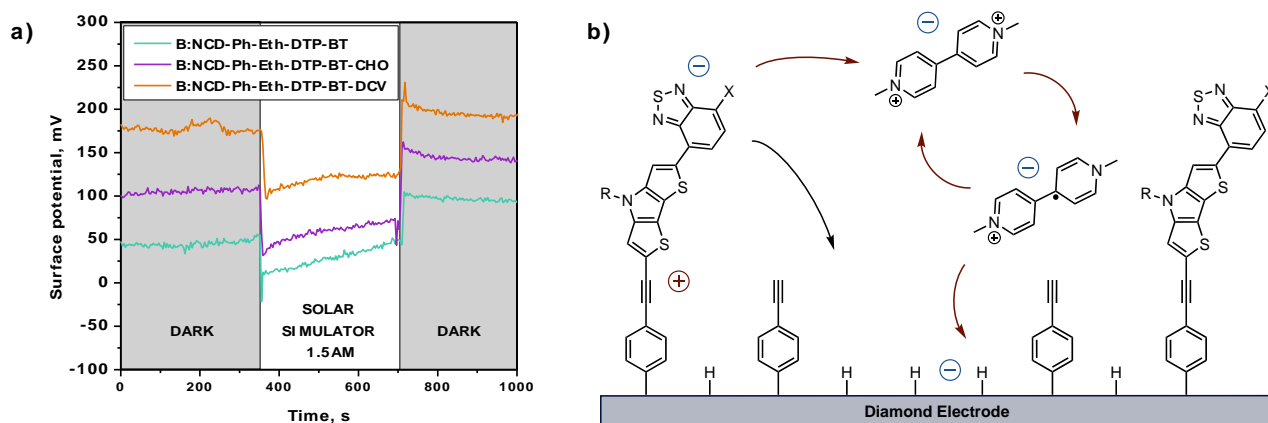
Figure 6 | a. Macroscopically measured surface potential profiles in the dark (shaded area) and under illumination (white area) for B:NCD electrodes functionalized with the three different chromophores. **b.** Schematic representation of the charge recombination that occurs for functionalized B:NCD electrodes. After excitation, electrons are first transferred to the methyl viologen redox electrolyte before charge recombination with the diamond electrode occurs.

4 Conclusions

In conclusion, we have established monolayer functionalized of boron-doped nanocrystalline diamond electrodes with ethynylphenyl molecules via the electrochemical diazonium grafting of 4-(trimethylsilyl)ethynylbenzenediazonium tetrafluoroborate. Monolayer formation on nanocrystalline diamond electrodes was confirmed by employing angular resolved XPS analysis. From the intensity of the B 1s peaks it was determined that the density of the grafted layer is controlled by the sterical hindrance of the trimethylsilyl protective groups, which likely results in small gaps in between the grafted molecules. Three types of dithienopyrrole-based iodinated organic donor-acceptor chromophores were then synthesized and immobilized onto the surface via Sonogashira cross-coupling reactions. The process leads again to monolayer, homogeneous chromophore coverage with negligible remaining impurities from the employed catalyst system. Atomic scale DFT calculations showed that among the investigated molecules the DTP-BT-DCV chromophore monolayer should provide superior photo-generated charge separation and injection to diamond based on the most suitable distribution of HOMO-LUMO orbitals, tight chromophore-diamond interaction in excited state transitions, and mutual energy level alignment. This was indeed confirmed by photovoltage and photoelectrochemical current measurements. The experimental and theoretically predicted trends were in a good agreement.

Yet, photocurrent and photovoltage measurements also indicated that after photoexcitation of the chromophore, the electrons were transferred to the redox electrolyte, but some were then regenerated at the diamond electrode instead of the counter electrode. This pathway seems to be unique for the monolayer functionalization approach and might be related to the gaps in the initially grafted layer of ethynylphenyl molecules. Although further research is required to suppress the electrolyte recombination mechanism (e.g. by additional surface passivation using various surface chemical groups or smaller

25

molecules), the presented approach with a monolayer of chromophores appears promising based on the achieved charge photogeneration and transport characteristics, especially in the case of DTP-BT-DCV.

Supporting information

The supporting information contains the computational analysis of excited states for the B:NCD-chromophore systems, additional information obtained by XPS after surface functionalization, a MALDI-ToF mass spectrum of the degradation product of DTP-BT-DCV in the presence of DIPA and ^{1}H/^{13}C NMR spectra of the DTP-BT, DTP-BT-CHO and DTP-BT-DCV chromophores.

Author Information

Corresponding Authors:

*E-mail: wouter.maes@uhasselt.be. Phone: +32-11-268312

*E-mail: rezekboh@fel.cvut.cz. Phone: +420-22435-2330

ORCID:

Jorne Raymakers: 0000-0003-1468-3108

Shannon S. Nicley: 0000-0002-5960-7873

Ken Haenen: 0000-0001-6711-7367

Wouter Maes: 0000-0001-7883-3393

Bohuslav Rezek: 0000-0002-0378-4598

Notes:

The authors declare that there is no conflict of interests.

Acknowledgements

References

[1] F.P. Bundy, H.T. Hall, H.M. Strong, R.H. Wentorf, Man-made diamonds, Nature, 176 (1955) 51-55.

[2] S. Yesudhas, F.P. Bundy, R.C. DeVries, Diamond: High-pressure synthesis, Elsevier, 2016.

[3] S. Matsumoto, M. Hino, T. Kobayashi, Synthesis of diamond films in a rf induction thermal plasma, Appl Phys Lett, 51 (1987) 737-739.

[4] M. Kamo, Y. Sato, S. Matsumoto, N. Setaka, Diamond synthesis from gas-phase in microwave plasma, J Cryst Growth, 62 (1983) 642-644.

[5] S. Matsumoto, Y. Sato, M. Tsutsumi, N. Setaka, Growth of diamond particles from methane-hydrogen gas, J Mater Sci, 17 (1982) 3106-3112.

[6] S.S. Nicley, S. Drijkoningen, P. Pobedinskas, J. Raymakers, W. Maes, K. Haenen, Growth of boron-doped diamond films on gold-coated substrates with and without gold nanoparticle formation, Cryst. Growth Des., 19 (2019) 3567-3575.

[7] L. Schafer, M. Hofer, R. Kroger, The versatility of hot-filament activated chemical vapor deposition, Thin Solid Films, 515 (2006) 1017-1024.

[8] S. Szunerits, Y. Coffinier, R. Boukherroub, Diamond nanowires: A novel platform for electrochemistry and matrix-free mass spectrometry, Sensors, 15 (2015) 12573-12593.

[9] H. Kato, J. Hees, R. Hoffmann, M. Wolfer, N. Yang, S. Yamasaki, C.E. Nebel, Diamond foam electrodes for electrochemical applications, Electrochem Commun, 33 (2013) 88-91.

[10] V. Petrák, Z. Vlčková-Živcová, H. Krýsová, O. Frank, A. Zukal, L. Klimša, J. Kopeček, A. Taylor, L. Kavan, V. Mortet, Fabrication of porous boron-doped diamond on SiO2 fiber templates, Carbon, 114 (2017) 457-464.

[11] T. Irifune, A. Kurio, S. Sakamoto, T. Inoue, H. Sumiya, Materials: Ultrahard polycrystalline diamond from graphite, Nature, 421 (2003) 599-600.

[12] K. Yoshida, H. Morigami, Thermal properties of diamond/copper composite material, Microelectron Reliab, 44 (2004) 303-308.

[13] C.H.Y.X. Lim, Y.L. Zhong, S. Janssens, M. Nesladek, K.P. Loh, Oxygen-terminated nanocrystalline diamond film as an efficient anode in photovoltaics, Adv. Funct. Mater., 20 (2010) 1313-1318.

[14] N. Y., Novel aspects of diamond: From growth to applications Springer, 2014.

[15] T.R. Rosa, F.S. Betim, R.D. Ferreira, Development and application of a labmade apparatus using open-source "arduino" hardware for the electrochemical pretreatment of boron-doped diamond electrodes, Electrochim. Acta, 231 (2017) 185-189.

[16] P.A. Nistor, P.W. May, Diamond thin films: Giving biomedical applications a new shine, J. R. Soc. Interface, 14 (2017) 20170382.

[17] J.B. Cui, J. Ristein, L. Ley, Electron affinity of the bare and hydrogen covered single crystal diamond (111) surface, Phys Rev Lett, 81 (1998) 429-432.

[18] J.V. Macpherson, A practical guide to using boron doped diamond in electrochemical research, Phys. Chem. Chem. Phys., 17 (2015) 2935-2949.

[19] K. Muzyka, J.R. Sun, T.H. Fereja, Y.X. Lan, W. Zhang, G.B. Xu, Boron-doped diamond: Current progress and challenges in view of electroanalytical applications, Anal Methods-Uk, 11 (2019) 397-414.

[20] T. Watanabe, K. Akai, Y. Einaga, The reduction behavior of free chlorine at boron-doped diamond electrodes, Electrochem Commun, 70 (2016) 18-22.

[21] T.A. Ivandini, Y. Einaga, Polycrystalline boron-doped diamond electrodes for electrocatalytic and electrosynthetic applications, Chem. Commun., 53 (2017) 1338-1347.

[22] A. Dirany, I. Sires, N. Oturan, A. Ozcan, M.A. Oturan, Electrochemical treatment of the antibiotic sulfachloropyridazine: kinetics, reaction pathways, and toxicity evolution, Environ. Sci. Technol., 46 (2012) 4074-4082.

[23] M. Tomisaki, S. Kasahara, K. Natsui, N. Ikemiya, Y. Einaga, Switchable product selectivity in the electrochemical reduction of carbon dioxide using boron-doped diamond electrodes, J. Am. Chem. Soc., 141 (2019) 7414-7420.

[24] S. Szunerits, C.E. Nebel, R.J. Hamers, Surface functionalization and biological applications of CVD diamond, MRS Bull., 39 (2014) 517-524.

[25] J. Raymakers, K. Haenen, W. Maes, Diamond surface functionalization: From gemstone to photoelectrochemical applications, J. Mater. Chem. C, 7 (2019) 10134-10165.

[26] H. Ye, L. Shen, S. Zhang, X. Li, F. Yu, R. Diao, J. Hua, Enhanced photocurrent via π-bridge extension of perylenemonoimide-based dyes for p-type dye-sensitized solar cells and photoelectrochemical cells, ACS Omega, 3 (2018) 14448-14456.

[27] P.-N. Volpe, J. Pernot, P. Muret, F. Omnès, High hole mobility in boron doped diamond for power device applications, Appl Phys Lett, 94 (2009) 092102.

[28] T. Strother, T. Knickerbocker, J.N. Russell, J.E. Butler, L.M. Smith, R.J. Hamers, Photochemical functionalization of diamond films, Langmuir, 18 (2002) 968-971.

[29] T.C. Kuo, R.L. McCreery, G.M. Swain, Electrochemical modification of boron-doped chemical vapor deposited diamond surfaces with covalently bonded monolayers, Electrochem Solid St, 2 (1999) 288-290.

[30] W.S. Yeap, D. Bevk, X. Liu, H. Krysova, A. Pasquarelli, D. Vanderzande, L. Lutsen, L. Kavan, M. Fahlman, W. Maes, K. Haenen, Diamond functionalization with light-harvesting molecular wires:

Improved surface coverage by optimized Suzuki cross-coupling conditions, RSC Adv., 4 (2014) 42044-42053.

[31] W.S. Yeap, X. Liu, D. Bevk, A. Pasquarelli, L. Lutsen, M. Fahlman, W. Maes, K. Haenen, Functionalization of boron-doped nanocrystalline diamond with N3 dye molecules, ACS Appl. Mater. Interfaces, 6 (2014) 10322-10329.

[32] H. Krysova, Z. Vlckova-Zivcova, J. Barton, V. Petrak, M. Nesladek, P. Cigler, L. Kavan, Visible-light sensitization of boron-doped nanocrystalline diamond through non-covalent surface modification, Phys. Chem. Chem. Phys., 17 (2015) 1165-1172.

[33] J. Raymakers, H. Krysova, A. Artemenko, J. Cermak, S.S. Nicley, P. Verstappen, S. Gielen, A. Kromka, K. Haenen, L. Kavan, W. Maes, B. Rezek, Functionalization of boron-doped diamond with a push-pull chromophore via Sonogashira and CuAAC chemistry, RSC Adv., 8 (2018) 33276-33290.

[34] S. Nakabayashi, N. Ohta, A. Fujishima, Dye sensitization of synthetic p-type diamond electrode, Phys. Chem. Chem. Phys., 1 (1999) 3993-3997.

[35] Y.L. Zhong, K.P. Loh, A. Midya, Z.-K. Chen, Suzuki coupling of aryl organics on diamond, Chem Mater, 20 (2008) 3137-3144.

[36] Y.L. Zhong, A. Midya, Z. Ng, Z.K. Chen, M. Daenen, M. Nesladek, K.P. Loh, Diamond-based molecular platform for photoelectrochemistry, J. Am. Chem. Soc., 130 (2008) 17218-17219.

[37] H. Krysova, L. Kavan, Z. Vlckova-Zivcova, W.S. Yeap, P. Verstappen, W. Maes, K. Haenen, F. Gao, C.E. Nebel, Dye-sensitization of boron-doped diamond foam: champion photoelectrochemical performance of diamond electrodes under solar light illumination, RSC Adv., 5 (2015) 81069-81077.

[38] J. Raymakers, A. Artemenko, S.S. Nicley, P. Štenclová, A. Kromka, K. Haenen, W. Maes, B. Rezek, Expanding the scope of diamond surface chemistry: Stille and Sonogashira cross-coupling reactions, J Phys Chem C, 121 (2017) 23446-23454.

[39] H. Krysova, J. Barton, V. Petrak, R. Jurok, M. Kuchar, P. Cigler, L. Kavan, Efficiency and stability of spectral sensitization of boron-doped-diamond electrodes through covalent anchoring of a donor-acceptor organic chromophore (P1), Phys. Chem. Chem. Phys., 18 (2016) 16444-16450.

[40] J. Bartoň, H. Krýsová, P. Janda, H. Tarábková, P. Ashcheulov, V. Mortet, A. Taylor, J. Vávra, P. Cígler, L. Kavan, Chemical modification of diamond surface by a donor–acceptor organic chromophore (P1): Optimization of surface chemistry and electronic properties of diamond, Appl. Mater. Today, 12 (2018) 153-162.

[41] P. Allongue, C.H. de Villeneuve, G. Cherouvrier, R. Cortes, M.C. Bernard, Phenyl layers on H-Si(111) by electrochemical reduction of diazonium salts: monolayer versus multilayer formation, J Electroanal Chem, 550 (2003) 161-174.

[42] J. Wang, M.A. Firestone, O. Auciello, J.A. Carlisle, Surface functionalization of ultrananocrystalline diamond films by electrochemical reduction of aryldiazonium salts, Langmuir, 20 (2004) 11450-11456.

[43] J. Pinson, F. Podvorica, Attachment of organic layers to conductive or semiconductive surfaces by reduction of diazonium salts, Chem. Soc. Rev., 34 (2005) 429-439.

[44] C. Jiang, S.M. Silva, S. Fan, Y. Wu, M.T. Alam, G. Liu, J.J. Gooding, Aryldiazonium salt derived mixed organic layers: From surface chemistry to their applications, J Electroanal Chem, 785 (2017) 265-278.

[45] H. Uetsuka, D. Shin, N. Tokuda, K. Saeki, C.E. Nebel, Electrochemical grafting of boron-doped single-crystalline chemical vapor deposition diamond with nitrophenyl molecules, Langmuir, 23 (2007) 3466-3472.

[46] S.Q. Lud, M. Steenackers, R. Jordan, P. Bruno, D.M. Gruen, P. Feulner, J.A. Garrido, M. Stutzmann, Chemical grafting of biphenyl self-assembled monolayers on ultrananocrystalline diamond, J. Am. Chem. Soc., 128 (2006) 16884-16891.

[47] Y.R. Leroux, H. Fei, J.M. Noel, C. Roux, P. Hapiot, Efficient covalent modification of a carbon surface: use of a silyl protecting group to form an active monolayer, J. Am. Chem. Soc., 132 (2010) 14039-14041.

[48] Y.R. Leroux, P. Hapiot, Nanostructured monolayers on carbon substrates prepared by electrografting of protected aryldiazonium salts, Chem Mater, 25 (2013) 489-495.

[49] H.I. Lu, C.W. Lu, Y.C. Lee, H.W. Lin, L.Y. Lin, F. Lin, J.H. Chang, C.I. Wu, K.T. Wong, New molecular donors with dithienopyrrole as the electron-donating group for efficient small-molecule organic solar cells, Chem Mater, 26 (2014) 4361-4367.

[50] Y. Fang, A.K. Pandey, D.M. Lyons, P.E. Shaw, S.E. Watkins, P.L. Burn, S.C. Lo, P. Meredith, Tuning the optoelectronic properties of nonfullerene electron acceptors, ChemPhysChem, 16 (2015) 1295-1304.

[51] P. Hohenberg, W. Kohn, Inhomogeneous Electron Gas, Phys. Rev., 136 (1964) B864-B871.

[52] W. Kohn, L.J. Sham, Self-Consistent Equations Including Exchange and Correlation Effects, Phys. Rev., 140 (1965) A1133-A1138.

[53] A.D. Becke, Density-functional exchange-energy approximation with correct asymptotic behavior, Phys. Rev. A, 38 (1988) 3098-3100.

[54] C. Lee, W. Yang, R.G. Parr, Development of the Colle-Salvetti correlation-energy formula into a functional of the electron density, Phys. Rev. B 37 (1988) 785-789.

[55] A.D. Becke, Density- functional thermochemistry. III. The role of exact exchange, J. Chem. Phys., 98 (1993) 5648-5652.

[56] E. Runge, E.K.U. Gross, Density-Functional Theory for Time-Dependent Systems, Phys Rev Lett, 52 (1984) 997-1000.

[57] T. Lu, F. Chen, Multiwfn: a multifunctional wavefunction analyzer, J. Comput. Chem., 33 (2012) 580-592.

[58] E. Touze, F. Gohier, S. Dabos-Seignon, T. Breton, C. Cougnon, A generic monolayer platform for the functionalization of surfaces through Sonogashira coupling, Synthetic Met, 247 (2019) 37-45.

[59] H. Zhou, L. Yang, W. You, Rational design of high performance conjugated polymers for organic solar cells, Macromolecules, 45 (2012) 607-632.

[60] P. Matunova, V. Jirasek, B. Rezek, DFT calculations reveal pronounced HOMO-LUMO spatial separation in polypyrrole-nanodiamond systems, Phys. Chem. Chem. Phys., 21 (2019) 11033-11042.

[61] A. Fujishima, Y. Einaga, N.T. Rao, D.A. Tryk, Diamond electrochemistry, 1ste ed., Elsevier, 2005.

[62] K. Natsui, T. Yamamoto, M. Akahori, Y. Einaga, Photochromism-induced amplification of critical current density in superconducting boron-doped diamond with an azobenzene molecular layer, ACS Appl. Mater. Interfaces, 7 (2015) 887-!894.

[63] R. Hoffmann, H. Obloh, N. Tokuda, N. Yang, C.E. Nebel, Fractional surface termination of diamond by electrochemical oxidation, Langmuir, 28 (2012) 47-50.

[64] T.A. Ivandini, T. Watanabe, T. Matsui, Y. Ootani, S. Iizuka, R. Toyoshima, H. Kodama, H. Kondoh, Y. Tateyama, Y. Einaga, Influence of surface orientation on electrochemical properties of boron-doped diamond, J Phys Chem C, 123 (2019) 5336-5344.

[65] T. Matsubara, M. Ujie, T. Yamamoto, M. Akahori, Y. Einaga, T. Sato, Highly sensitive detection of influenza virus by boron-doped diamond electrode terminated with sialic acid-mimic peptide, Proc. Natl. Acad. Sci. USA, 113 (2016) 8981-8984.

[66] V.A. Naumkin, A. Kraut-Vass, W.S. Gaarenstroom, J.C. Powell, NIST x-ray photoelectron spectroscopy database, in, 2012.

[67] T. Yamamoto, M. Akahori, K. Natsui, T. Saitoh, Y. Einaga, Controlled decoration of boron-doped diamond electrodes by electrochemical click reaction (e−CLICK), Carbon, 130 (2018) 350-354.

[68] M. Wang, M.R. Das, M. Li, R. Boukherroub, S. Szunerits, "Clicking" thiophene on diamond interfaces. Preparation of a conducting polythiophene/diamond hybrid material, J Phys Chem C, 113 (2009) 17082-17086.

[69] J. Kesters, P. Verstappen, J. Raymakers, W. Vanormelingen, J. Drijkoningen, J. D'Haen, J. Manca, L. Lutsen, D. Vanderzande, W. Maes, Enhanced organic solar cell stability by polymer (PCPDTBT) side chain functionalization, Chem Mater, 27 (2015) 1332-1341.

[70] T.E. Barder, S.D. Walker, J.R. Martinelli, S.L. Buchwald, Catalysts for Suzuki-Miyaura coupling processes: scope and studies of the effect of ligand structure, J. Am. Chem. Soc., 127 (2005) 4685-4696.

[71] J.R. Naber, S.L. Buchwald, Palladium-catalyzed Stille cross-coupling reaction of aryl chlorides using a pre-milled palladium acetate and XPhos catalyst system, Adv. Synth. Catal., 350 (2008) 957-961.

[72] W.P. Gallagher, A. Vo, Dithiocarbamates: Reagents for the removal of transition metals from organic reaction media, Org. Process Res. Dev., 19 (2014) 1369-1373.

[73] D. Hirayama, K. Takimiya, Y. Aso, T. Otsubo, T. Hasobe, H. Yamada, H. Imahori, S. Fukuzumi, Y. Sakata, Large photocurrent generation of gold electrodes modified with [60]fullerene-linked oligothiophenes bearing a tripodal rigid anchor, J. Am. Chem. Soc., 124 (2002) 532-533.

[74] T. Otsubo, Y. Aso, K. Takimiya, Functional oligothiophenes as advanced molecular electronic materials, J Mater Chem, 12 (2002) 2565-2575.